Oxidation of NiAl(110)
by Wade William Brown

A thesis submitted in partial fulfillment of the requirements for the degree of Master of Science in Physics
Montana State University
© Copyright by Wade William Brown (1990)

Abstract:
We have studied the oxidation of NiAl(110) using Auger electron spectroscopy, x-ray photoelectron spectroscopy, surface second harmonic generation measurements, and contact potential difference measurements. Oxygen forms a bond to the aluminum atoms on the (110) surface, although the oxide formed is geometrically and possibly chemically different from' that formed in Al2O3. The adsorbed oxygen is weakly incorporated into the surface, having a sticking coefficient very much smaller than that found on any low index aluminum surface. There is little or no direct interaction between the nickel atoms in the surface region and the adsorbed oxygen. Instead, nickel serves indirectly to stabilize the surface against oxygen adsorption through the nickel-aluminum bonding of the substrate. There is no evidence that nickel is depleted in the surface region by the oxygen adsorption process. The oxide that forms under heavy exposures forms first on top of the surface and subsequently diffuses into the bulk.

OXIDATION OF NIAL(110)

by

Wade William Brown

A thesis submitted in partial fulfillment
of the requirements for the degree

of

Master of Science

in

Physics

MONTANA STATE UNIVERSITY
Bozeman, Montana

July, 1990

N378
B8164

APPROVAL

of a thesis submitted by

Wade William Brown

This thesis has been read by each member of the thesis committee and has been found to be satisfactory regarding content, English usage, format, citations, bibliographic style, and consistency, and is ready for submission to the College of Graduate Studies.

4 Aug 90
Date

Chairperson, Graduate Committee

Approved for the Major Department

8-14
Date

Head, Major Department

Approved for the College of Graduate Studies

August 15, 1990
Date

Graduate Dean

STATEMENT OF PERMISSION TO USE

In presenting this thesis in partial fulfillment of the requirements for a master's degree at Montana State University, I agree that the Library shall make it available to borrowers under rules of the Library. Brief quotations from this thesis are allowable without special permission, provided that accurate acknowledgment of source is made.

Permission for extensive quotation from or reproduction of this thesis may be granted by my major professor, or in his/her absence, by the Dean of Libraries when, in the opinion of either, the proposed use of the material is for scholarly purposes. Any copying or use of the material in this thesis for financial gain shall not be allowed without my written permission.

Signature _____

Date August 3, 1990

ACKNOWLEDGEMENTS

I would like to thank the members of my committee Dr. John L. Carlsten and Dr. Adolfo G. Eguiliz who read through this thesis carefully and offered suggestions. Dr John L. Carlsten's expertise in the area of lasers was extremely beneficial to my second harmonic generation measurements. Also, I would like to thank the staff of the CRISS facility here at Montana State University, Dr. James R. Anderson and Milton Jaehnig. They assisted my research efforts while making measurements in the CRISS facility and also assisted me when making measurements in our laboratory.

Finally, I would like to thank my advisor Dr. Wayne K. Ford, who supplied an environment that allowed me to learn about a wide range of topics in surface science. Dr. Ford also read through this thesis in its early stages and offered a great deal of help and insight.

TABLE OF CONTENTS

Page

APPROVAL ii

TABLE OF CONTENTS v

LIST OF FIGURES vi

ABSTRACT viii

CHAPTERS

1. INTRODUCTION 1

2. EXPERIMENTAL TECHNIQUES 4

   Sample Preparation 4

   Auger Electron Spectroscopy 9

   X-Ray Electron Spectroscopy 15

   Kelvin Probe 18

   Surface Second Harmonic Generation 23

3. PREVIOUS OXIDATION STUDIES 28

   Oxidation of Aluminum 28

   Oxidation of Nickel 35

   Oxidation of Nickel Aluminum 39

4. EXPERIMENTAL RESULTS FOR NICKEL ALUMINUM 41

5. DISCUSSION OF RESULTS 54

REFERENCES CITED 63

LIST OF FIGURES

Figure Page

1. Modified PHI 545 Ultra High Vacuum Chamber 7
2. Sample Holder for Modified PHI 545 Chamber 8
3. Auger decay process 10
4. Auger cross section for oxygen on aluminum versus Ep/E 13
5. Schematic of x-ray photoemission process 16
6. Double charge layer 19
7. Contact potential difference capacitor circuit 21
8. Drawing of Kelvin probe assembly 22
9. Optical setup for SHG experiment 26
10. Electronics schematic for SHG experiment 27
11. Three low index faces for face centered cubic lattice 29
12. Work function change versus oxygen exposure for aluminum 33
13. AES oxygen uptake for aluminum 35
14. Work function change versus exposure for Ni(100) 37
15. Oxygen uptake for Ni(111) 38
16. Oxygen uptake for Ni(100) 39
17. Top view of the NiAl(110) surface 41
18. Proposed two layered rippled surface for NiAl(110) 42
19. Representative Auger spectra from PHI 595 44
20. Normalized Auger peak heights versus O2 exposure for NiAl(110) 45
21. Low energy aluminum and nickel Auger peaks versus exposure 47

LIST OF FIGURES – Continued

Figure Page

22. Work function change versus exposure for clean surface 49

23. Work function change versus exposure for a contaminated surface 50

24. Second harmonic intensity versus exposure 51

25. XPS spectra for Ni 2p core levels versus oxygen exposure 52

26. XPS spectra for Al 2p and Ni 3p core levels versus exposure 53

27. Atomic concentration versus exposure 60

28. Saturation atomic concentration versus oxygen exposure 62

ABSTRACT

We have studied the oxidation of NiAl(110) using Auger electron spectroscopy, x-ray photoelectron spectroscopy, surface second harmonic generation measurements, and contact potential difference measurements. Oxygen forms a bond to the aluminum atoms on the (110) surface, although the oxide formed is geometrically and possibly chemically different from that formed in Al_2O_3. The adsorbed oxygen is weakly incorporated into the surface, having a sticking coefficient very much smaller than that found on any low index aluminum surface. There is little or no direct interaction between the nickel atoms in the surface region and the adsorbed oxygen. Instead, nickel serves indirectly to stabilize the surface against oxygen adsorption through the nickel-aluminum bonding of the substrate. There is no evidence that nickel is depleted in the surface region by the oxygen adsorption process. The oxide that forms under heavy exposures forms first on top of the surface and subsequently diffuses into the bulk.

CHAPTER 1

INTRODUCTION

The physical properties of intermetallic alloys such as the transition metal aluminides were extensively studied first during the 1950's and 1960's and interest in these materials have continued to this day.[1] Early on many attractive properties were found: high strength at high temperatures, high corrosion resistance, and high ductility for single-crystal specimens, to name a few. In recent years with the advent of modern surface science techniques a new interest in the surface properties of the intermetallic alloys has occurred. These more microscopic tools have allowed scientists to study both bulk properties and surface phenomena with considerably greater control and reliability.

Of the intermetallic alloys, the nickel aluminides have many fundamentally interesting and technologically useful properties. The bulk properties of this family of materials stand out. For example, the yield strength of conventional alloys, such as stainless steel, decrease with increasing temperature. However, Liu and Stiegler showed for Ni_3Al+0.2B the yield strength actually increases up to a temperature of about 600°C.[1] The reason for the high temperature strength of Ni_3Al is thought to be associated with the process of microalloying.[1] Microalloying is a metallurgical technique of adding small concentrations of compounds in order to enhance certain desirable properties. For the case cited above, microalloying of Ni_3Al with boron not only increases its high temperature strength but also increases its ductility by 50% over that measured for pure Ni_3Al.[2] This is very important to technological applications of the material because the ductility of a material determines the ease by which it can be machined.

The surface chemistry of the nickel aluminum alloys is also of technological interest because these alloys can be used as corrosion resistant materials and as heterogeneous catalysts. The application of nickel aluminum as a corrosion resistant material is technologically important because of the wide spread desire for the long term stability of products to degradation due to corrosion. The application of nickel aluminum as a heterogeneous catalyst is of technological importance because one-sixth of the value of all goods manufactured in the United States involve catalytic processes. Recent research in this area has shown that mixed-metal catalysts can provide a powerful way to control catalytic activity and selectivity.[3]

Notwithstanding their technological potential, the nickel aluminides offer the basic scientist a special family of materials with which to study the electronic structure of metals and metallic surfaces. There are at least three ordered stoichiometries of nickel aluminum: Ni_3Al, NiAl, and $NiAl_3$. Each represents a blend of a classic simple metal with the archetypal d-band transition metal in an ordered, characterizable lattice. The relative importance of the d-band atom to the electronic, geometric, and chemical properties of the bulk alloy can be examined by comparing materials of different stoichiometries. For each stoichiometry the properties of the bands derived from the nickel 3d shell electrons will reflect both lattice and hybridization effects, the latter being due to the alloy bonding of the nearly free aluminum electrons. Heuristically speaking, the d-bands are filled as the aluminum content is increased. This is accomplished without the addition of any new d-states, as one would have, for example, in nickel copper alloys. In addition to the several bulk stoichiometries, each low index face of the crystal isolates a different relative surface composition of the aluminum and nickel atoms or presents a different aluminum-nickel intra-plane spacing. One expects that these geometric considerations will be manifest in dramatic effects in the surface electronic structure and surface chemical activity of the material.

NiAl(110) is a good choice as a model surface for experimental and theoretical studies of the surface chemical properties of the nickel aluminum alloys because it forms a stable, 50-50 stoichiometry on a microscopic scale. Our work investigates the incipient oxidation of this surface. We have sought to characterize the oxidation of NiAl(110) in the "monolayer" regime and to draw distinctions between this alloy and the oxidation properties of the more familiar aluminum and nickel surfaces. In Chapter 2 a description of the experimental methods and techniques used in the study is presented. In Chapter 3 we review what is known about the oxidation of aluminum and nickel. Our experimental results are presented in Chapter 4, and we conclude with our interpretation of those results in Chapter 5.

CHAPTER 2

EXPERIMENTAL TECHNIQUES

No one experimental probe is generally sufficient to characterize the surfaces of materials. In surface science one is forced to utilize a wide variety of techniques to address a problem. In this study of nickel aluminum x-ray photoelectron spectroscopy (XPS), Auger electron spectroscopy (AES), Kelvin probe work function analysis ($\Delta\phi$), laser second harmonic generation (SHG), and elastic low energy electron diffraction (LEED) measurements were performed using equipment in the surface science laboratories at Montana State University. In this chapter the application of these techniques and their underlying physical principles are discussed. First, the preparation of the sample is described.

Sample Preparation

The nickel aluminum single crystal was obtained from Dr. D. Zehner of Oak Ridge National Laboratory and Dr. D. Pease of the University of Connecticut. Prior to our measurements the sample orientation was checked by the method of Laue x-ray diffraction. The crystal surface orientation was determined to be within 0.5° of the (110) plane. Mechanical polishing of the (110) surface was performed by using successively finer grades of alumina polish, starting out with a 5 μ polish and finishing with a 0.05 μ polish. This sequence of polishing steps produced a surface with little light scatter when checked with a helium neon laser. A minimum amount of light scatter from the surface is important for the success of the SHG experiment. In later measurements we found that a

better optical surface could be obtained with a final polish of Syton,* a silicon based colloidal suspension. Polishing with Syton reduced further the light scatter from the surface, but changed somewhat the work function measurements. As described below, although the total change in work function with oxygen exposure was reproducible between preparation methods, the Syton polished sample reached a saturation value at a slightly lower exposure. After mechanical polishing the sample was ultrasonically cleaned in a bath of acetone, followed by a rinse of methanol.

In ultra-high vacuum the crystal was cleaned by repeated cycles of high-temperature sputtering at a sample temperature of 850°C, followed by a ten minute anneal at 850°C. No effect of cooling rate after the anneal was observed in our measurements. The sputtering was done at a primary ion beam energy of 800 eV to 1000 eV for fifteen minutes each cycle. The anneal was necessary to remove any damage done to the surface during sputtering, and, in particular, to restore the 50-50 stoichiometry of the bulk to the surface since aluminum is preferentially sputtered from nickel aluminum.[4] The sample was considered clean when there was no detectable Auger signal from carbon or oxygen contamination. In one chamber XPS was used to establish cleanliness. In this case signal averaging was used to increase the signal to noise ratio because the cross section for x-ray ionization for these two elements is small at the available photon energies. In the other two systems surface contamination checking was done with AES. It usually took only one sputter-anneal cycle to clean the sample.

The experiments were performed using three separate ultrahigh vacuum chambers. Oxygen uptake measurements were carried out primarily in a Physical Electronics Scanning Auger Microprobe (SAM) model PHI 595. This system was equipped with a Digital Equipment PDP-11 computer that controlled a single pass cylindrical

---

* Remet Chemical Corp. 278 Chadwicks, N.Y. 13319

mirror analyzer (CMA) and performed data acquisition. The CMA is an energy band pass dispersive device used to measure the kinetic energy distribution of the Auger electrons. The ultra-high vacuum chamber of the 595 was pumped by an ion pump, a titanium sublimation pump, and a turbo pump. The working pressure of this system was around 5 x 10^{-10} Torr. The sample was held in place using the holder provided with the machine.

Other AES measurements were carried out in a modified commercial chamber, a Physical Electronics model 545, equipped as above with a single pass CMA with integral gun. A schematic of this chamber is presented in Figure 1. The AES measurements carried out in this chamber were made to monitor surface condition prior to Kelvin probe and second harmonic measurements. This chamber was also equipped with a low energy electron diffraction (LEED) apparatus and a Kelvin probe for measuring work function changes. This was the chamber in which the second harmonic generation measurements were performed. The single pass CMA was computer controlled using an ATT 6300+ microcomputer. An experimental control system was developed by adapting a general purpose experimental control program written for the ATT computer by Will Hough, an MSU undergraduate research assistant. The computer programs controlled all of the experiments performed in this chamber. This system included an ion sputter gun for sample preparation. The chamber was pumped by an ion pump, a titanium sublimation pump, and a turbo pump, which provided a working pressure of this system of around 2 x 10^{-10} Torr.

A third chamber, manufactured by Leybold Heraeus, was used for the XPS measurements. The vacuum was maintained with two ion pumps, two turbo pumps, and a titanium sublimation pump. The working pressure was around 1 x 10^{-10} Torr. Included with the chamber was a electron energy loss spectrometer, a dual anode x-ray source, and a

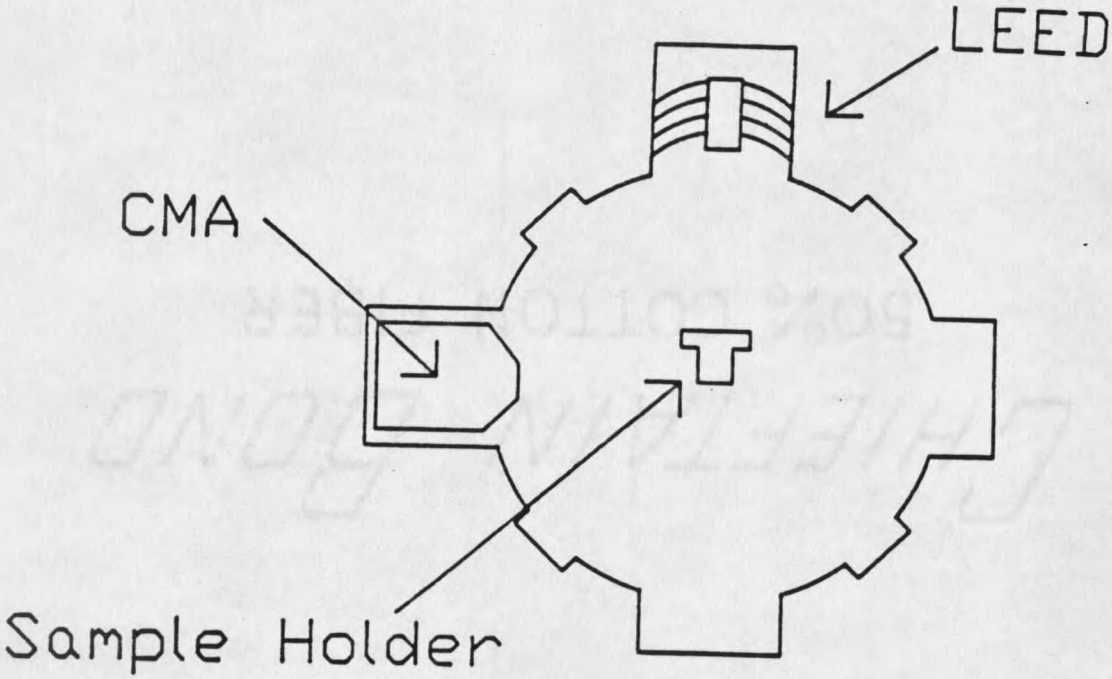

Figure 1: Modified PHI 545 Ultra High Vacuum Chamber.

hemispherical energy analyzer. Sample preparation was performed with an ion sputter gun.

A different sample holder was used for each of the three chambers used. The sample holder used in the modified 545 chamber is displayed in Figure 2. It was designed to maintain the position of sample during heating. This was important because the SHG measurements required the surface plane of the sample to remain in a constant position so as not to disturb the optical alignment of the laser and detection optics positioned outside of the vacuum vessel. The nickel aluminum crystal was machined to have a raised surface which allowed for secure mounting using a stainless steel 0.010 inch face plate. The face plate did not extend above the sample surface. Thus, shadowing effects were eliminated when the sample was cleaned using sputter ion bombardment. The sample holder was

hollowed out to form a space behind the sample. Inside this cavity was a 0.010 inch tantalum filament used as an electron source for electron bombardment heating. The sample was held at ground potential and the filament floated at a negative potential for heating. This heating arrangement gave good temperature control from 200°C to 850°C. The temperature was monitored with a chromel-alumel thermocouple. The sample was customarily heated from room temperature to 850°C in less than five minutes.

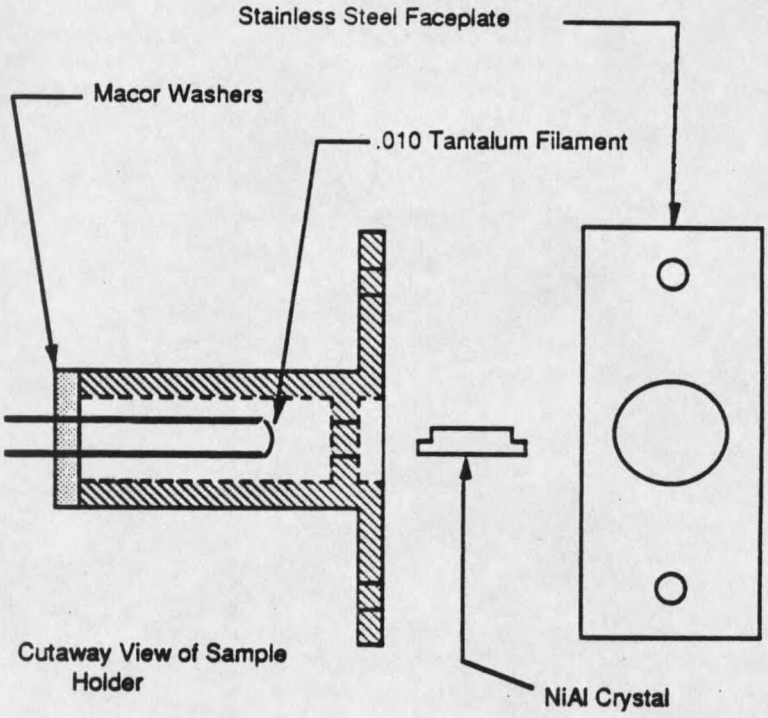

Figure 2: Sample Holder for Modified PHI 545 Chamber

In the XPS chamber the sample was mounted between two pieces of .010 inch tantalum foil. The tantalum foil pieces had holes cut out of them with the same diameter as the raised surface on the crystal. The crystal was placed between the two foil pieces, with the raised surface of the sample protruding through one of the foil pieces. Then the foil pieces were spot welded together. The foil and sample arrangement were mounted on the spectrometer manipulator over a .010 inch tantalum filament which served as an electron

source. The temperature was monitored with a platinum-platinum rhodium 10% alloy thermocouple spot welded to the sample.

Auger Electron Spectroscopy

Auger electron spectroscopy is used routinely by surface scientists to quantify the elemental composition of surfaces. A high energy beam of electrons with kinetic energies in the range of 1 keV to 10 keV is made to strike a sample surface. The penetrating beam undergoes both elastic and inelastic collisions, losing most of its energy over a depth of 10 to 20 Å.[5] Core level electrons are ejected during collisions with the atoms of the material, leaving a trail of ions and atoms in various excited states which will decay to lower energy configurations with an emission of either a photon via x-ray fluorescence or an electron in an Auger process. The probability for x-ray emission falls off with lower atomic number and more shallow core levels. For lighter elements and shallow cores Auger emission is favored over fluorescence. An empirically derived relation giving the transition probability ω for fluorescence is given by $\omega = (1 + aZ^4)^1$ where the constant 'a' has a value of 1.12×10^6 for K shell ionizations and 6.4×10^7 for L shell processes.[6] For example, from this expression the photon transition probability is 3.2% for L shell ionizations in strontium and 3.3% for K shell ionizations in silicon. Thus, as a practical matter incident electrons with 2 keV kinetic energy will not produce appreciable x-ray fluorescence from the K, L, and M atomic shells below atomic numbers of 14 (silicon), 38 (strontium), and 76 (osmium), respectively.

A schematic view of the Auger de-excitation process is presented in Figure 3. The ejected electrons come from a core level of binding energy ε_1 relative to the chemical potential. An electron from an outer shell of binding energy ε_2 subsequently relaxes into the vacancy in the core level. The energy released in this transition is taken up by a third

electron of energy ε_3 which is subsequently ejected from the material. This second ejected electron is called the Auger electron. The vacuum kinetic energy of this electron E_A is given, neglecting electron correlation, by $E_A = \varepsilon_1 - \varepsilon_2 - \varepsilon_3 - W$ where W is the work function of the material. Note that the final state of this process leaves the atom in a two-hole ionized state that can subsequently relax via Auger emission with the valence electrons.

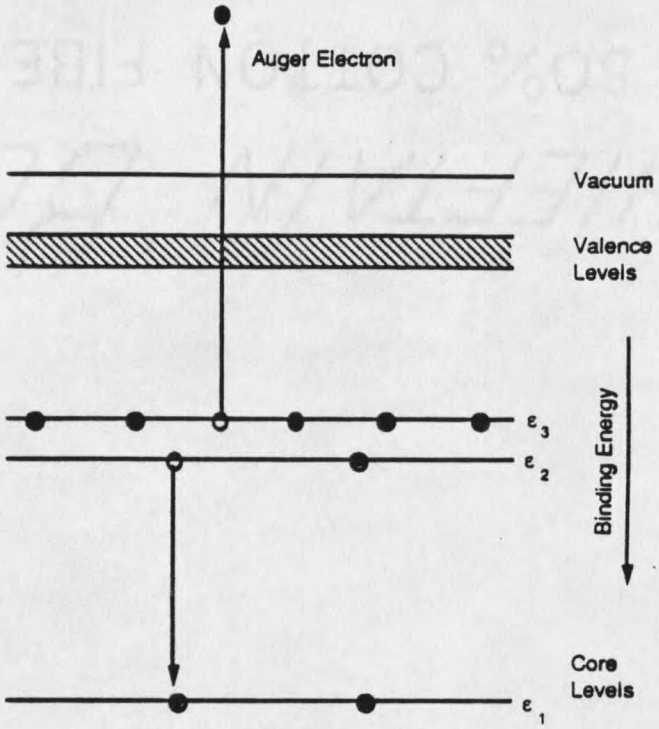

Figure 3: Auger decay process

A more complete understanding of the Auger process requires one to examine ionization cross sections and backscattering factors. Ionization cross sections give the probability of ionization for an electron atom scattering event. The backscattering factor gives a measure of the number of Auger secondary electrons that will undergo additional scattering events prior to being emitted from the sample. Ionization cross sections have been estimated previously[7] and the total cross section $\sigma(E_p)$ was given as

$$\sigma(E_p) = \frac{2\pi e^2}{E_p E} b \ln \frac{4E_p}{B}$$

Here E_p is the energy of the incident primary electrons, E is the ionization potential, e is the charge on the electron, b is equal 0.35 for K shell electrons and 0.25 for L shell electrons, and B is a function of E_p and E. Worthington and Tomlin[8] found B to have the following form for $E \leq E_p$:

$$B = \left\{ 1.65 + 2.35 \exp\left(1 - \frac{E_p}{E} \right) \right\} E$$

They arrived at this form of B empirically by requiring that $\sigma(E_p)$ would vanish at E_p equal to E and that the shape would be the same as had been shown experimentally. Combining these results yields

$$\sigma(E_p) = 1.3x10^{-13} \frac{b}{UE^2} \ln \left\{ \frac{4U}{1.65 + 2.35(1-U)} \right\} (cm^2)$$

where U equals E_p/E.

The result for $\sigma(E_p)$ should also be corrected to include the effect of multiply scattered and backscattered electrons. The correction term is given by

$$\sigma' = \int_E^{E_p} \sigma(E)\ n(E)\ dE$$

where n(E) is the number of backscattered electrons at energy E. This correction term can be combined with $\sigma(E_p)$ to give the total corrected cross section

$$\sigma'(E_p) = \sigma(E_p)\{1 + r_m(E_p, E, \alpha)\}$$

where $r_m(E_p,E,\alpha)$ is the correction due to the backscattered electrons. The term $r_m(E_p,E,\alpha)$ is dependent on both the incident and ionization energies and the matrix in which the atoms are embedded, denoted by α. Reuter[9] has empirically determined a relationship for the backscattering term. The relationship is

$$r_m(E_p, E) = 1 + 2.8\eta\left(1 - 0.9\frac{E_p}{E}\right).$$

η is a material dependent parameter and is given in terms of atomic number by

$$\eta = -0.1254 + 0.016\,Z - 0.000186\,Z^2 + 8.3 \times 10^{-7}\,Z^3.$$

In the case of aluminum (Z = 13) the backscattering correction term $r_m(E_p,E,\alpha)$ is equal to 1.08 for $E/E_p = 0.5$.

Figure 4 is a graph of σ and σ' versus E_p/E for the specific case of oxygen on a substrate of aluminum. The dependance of the cross section on the adatom is through the ionization energy for the adatom. By examining the figure it is seen that the σ' reaches a maximum at about E_p/E equal to about 2.6. Therefore, to maximize the probability of an oxygen Auger transition the primary energy of the beam should 2.6 times the ionization energy of the oxygen level of interest, in this case 532 eV. The backscattering term increases the cross section at the maximum nearly a factor of two, due to the additional Auger transitions induced by the backscattered electrons.

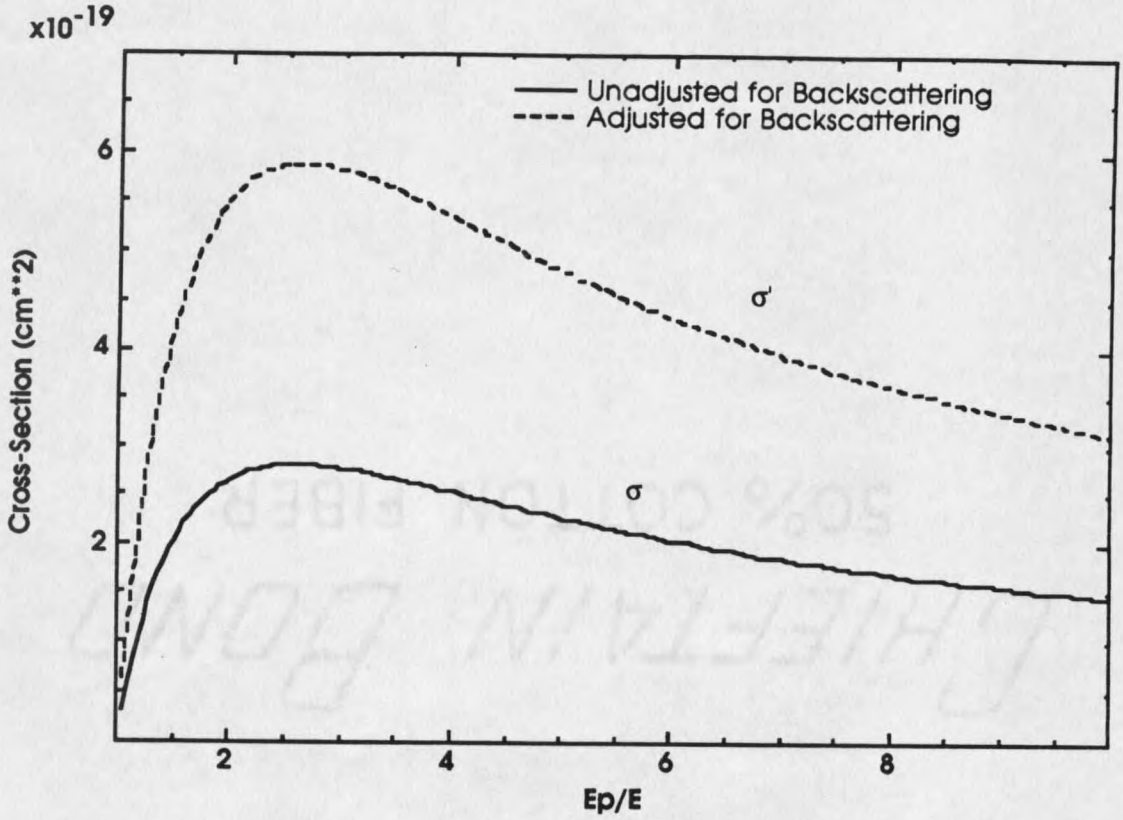

Figure 4: Auger cross section for oxygen on aluminum versus E_p/E

It is informative to illustrate the difficulties involved with performing submonolayer detection using AES. Consider the oxygen Auger current from .01 monolayers (Θ = .01) of adsorbed oxygen on a substrate of aluminum. For a coverage of N atoms/cm^2, the probability of an Auger transition per incident electron is given by

$$n = N\sigma'(E_p).$$

The number of sites available on the aluminum surface for oxygen is about 10^{15}/cm^2. Therefore, with a coverage of .01 monolayers N = 10^{13}/cm^2. The K shell in oxygen has an ionization energy of 532 eV. With a beam of primary energy of 2 keV the Auger cross

section is approximately $2x10^{-19}$ cm^2. This leads to a transition probability of $2x10^{-6}$. Therefore, the oxygen transition of interest here has a relative sensitivity of about 10^{-6}. The Auger current produced by this transition will be the probability of a transition times the current of the incident beam. For this example assume a beam current of $1x10^{-6}$A then the Auger current produced will be equal to about 2×10^{-12} A. This current will be emitted over a solid angle of 4π steradians. The current collected by the analyzer will be reduced due to the fact that the analyzer cannot collect over the full solid angle, the collected current will be reduced by a factor of $\Omega/4\pi$, where Ω is the solid angle subtended by the analyzer. The solid angle of our analyzer is about 0.75 steradians, yielding a current at the analyzer of about 1×10^{-13} A. Thus, the electron analyzer has to have an absolute sensitivity of about 10^{-13} in order to detect an oxygen coverage of .01 monolayer on a substrate of aluminum. Detection of this signal is further complicated by the fact that Auger current will be added to a background signal produced by secondary electrons 10^6 times as large. Since the background current is a slowly varying function of kinetic energy the detection of the Auger peaks is customarily enhanced by differentiating the total signal with respect to the energy. This is either done numerically or by applying an oscillating voltage to the analyzer and utilizing lock-in amplifier techniques.

The mean free path of the Auger electrons must be considered when analyzing Auger data. The mean free path is defined as the distance required to attenuate the Auger electron signal by a factor of e^{-1}. It is kinetic energy dependent and ranges from about 4Å to 40 Å over the primary electron energy range used most commonly.[10] The mean free path in metals reaches a minimum at an electron energy of about 40 eV. Auger electrons with a short free mean path will be most surface sensitive. The sampling depth of any measurement will be determined by the mean free path of the *escaping* electrons and will therefore vary with the atomic core shells being studied. Thus, each line in a spectrum emanates from a different volume of the sample surface region.

Whereas the interpretation of Auger spectroscopy from elemental substrates is well advanced, it is far less developed for composite and alloy materials. In the case of chemisorption systems, the interaction of the adsorbate and the substrate must be included when estimating cross-sections. However, non-uniform core level shifts and, more importantly, hybridization of the valence electrons which occur in chemisorption systems will modify the Auger cross-sections. Geometrical changes can also make important modifications to the backscattering corrections. In the case of pure alloys the cross-section measurements will differ from the pure element case and have not been performed for a large number of systems. Finally, with particular relevance to the work described herein, the problem of estimating cross-sections for chemisorption systems involving alloys has hardly been addressed. Hence, the Auger signal strengths can only approximately be used to examine concentrations of adsorbed species on alloy surfaces.

X-Ray Photoelectron Spectroscopy

Photoelectron spectroscopy is a powerful tool for the characterization and study of surfaces. When a solid is irradiated with x-rays, photoelectrons are produced and emitted from the solid. The kinetic energy of these electrons is given by $E = h\nu - \varepsilon - W$ where $h\nu$ is energy of the incident x-ray, ε is the binding energy of the atomic orbital and W is the work function of the solid. Figure 5 gives a graphical representation of this process. Sample illumination by monochromatic sources of x-rays will emit photoelectrons with discrete energies corresponding to unique atomic core levels. The elemental fingerprinting of surface atomic species using x-rays in this manner is called x-ray photoelectron spectroscopy or XPS.

The sampling depth for XPS is determined by two things: the dielectric constant of the material and the mean free path of the photoelectrons. The dielectric constant describes

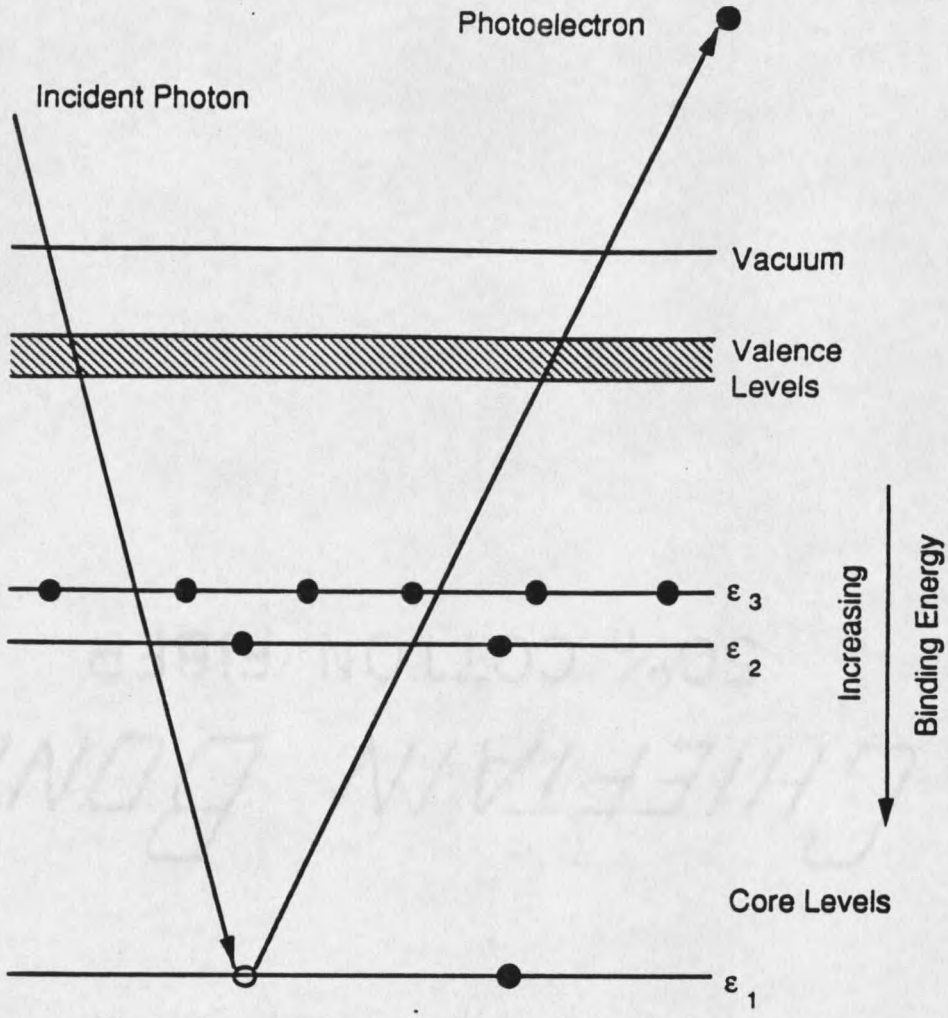

Figure 5: Schematic of x-ray photoemission process

the optical response of the materials and is complex-valued over at least one range of ν, the optical frequency. The optical response involves collective excitations, such as plasmons and shake-up, and single-particle excitations. The imaginary part of the dielectric constant leads to attenuation, thereby limiting the penetration of the radiation field into the substrate to a few hundred Ångstöms, typically. On the other hand, the probability of interaction of the photoelectron with the substrate is much greater. Because the typical mean free path of the photoelectrons is of the order of ten Ångstöms the photoelectron mean free path, or escape depth, is the dominant factor in determining the sampling depth.

The XPS measurements presented here were performed in a Leybold Hereaus (L-H) ultrahigh vacuum chamber, equipped with an L-H dual anode x-ray gun. The x-rays produced by this x-ray gun are not completely monochromatic due to bremsstrahlung scattering, satellite peaks, and the natural line width of the fluorescing core hole states. However, for our purposes the x-rays were used without further monochromatization. The two target elements provided with this gun were aluminum and magnesium having photon energies (and linewidths) of 1486.6 eV (0.85 eV) and 1253.6 eV (0.7 eV), respectively. Because, the aluminum anode could be operated at a higher power, level it was used when checking for carbon and oxygen contamination, whose relatively small x-ray cross-sections at the available photon energies render their detection at submonolayer concentrations difficult. The magnesium anode was used when studying core level shifts because the Mg K_α line has a narrower line width and, thus, provided higher resolution than the Al K_α line.

The photoelectrons were analyzed using a 12.5 cm mean radius hemispherical capacitor spectrometer, an L-H model EA11. The analyzer was run in the constant pass energy mode with a pass energy of 35 eV or 75 eV, selected depending on the measurement being made. The pass energy was selected according to the measurement being made. When checking for contaminants (predominantly carbon and oxygen), the pass energy was set to the larger value of 75 eV. A large pass energy provides a larger analyzer transmission which is needed for detection of carbon and oxygen due to the low instrumental sensitivities to these elements. The analyzer was run at a pass energy of 35 eV when scanning the structure of the nickle and aluminum core levels. The system was controlled and data collected using a Tektronix model 4052 microcomputer.

Kelvin Probe

The work function of a material is defined as the minimum energy required to free an electron from a solid. If the charge distribution on the surface were to reproduce that within the bulk, the work function would be equal to the negative of the Fermi energy. However, this is not usually the case. The difference in the surface distribution can be modeled as a uniform macroscopic surface dipole density. This surface dipole density is often termed the double layer.[11] Figure 6 gives a diagram of this. The double charge layer is affected by many things, for example, crystal orientation, adsorbed molecules, and surface condition. To obtain a correct expression for the work function the amount of energy required to move a test charge through this double layer must be added to the negative of the Fermi energy.

Bringing two isolated metals of different work functions into contact will cause a transfer of charge to equilibrate the combined system. This transfer of charge occurs because of the difference in chemical potentials for electrons, or Fermi levels, between the two isolated metals. The potential difference is known as the Contact Potential Difference or CPD and is equal to the difference in work functions. The Kelvin Probe method of measuring work functions exploits this property directly.

One can understand the Kelvin Probe method as follows. Assume that two dissimilar metals form a parallel plate capacitor. There will be a surface charge density formed on the opposing plates because of the CPD. The equation for the charge Q on this capacitor is $Q = CV_C$ where C is the capacitance and V_C is the contact potential difference. To perform the work function measurement it is useful to vary the distance between the capacitor plates. Varying the distance in a sinusoidal fashion allows one to measure easily an alternating current signal.

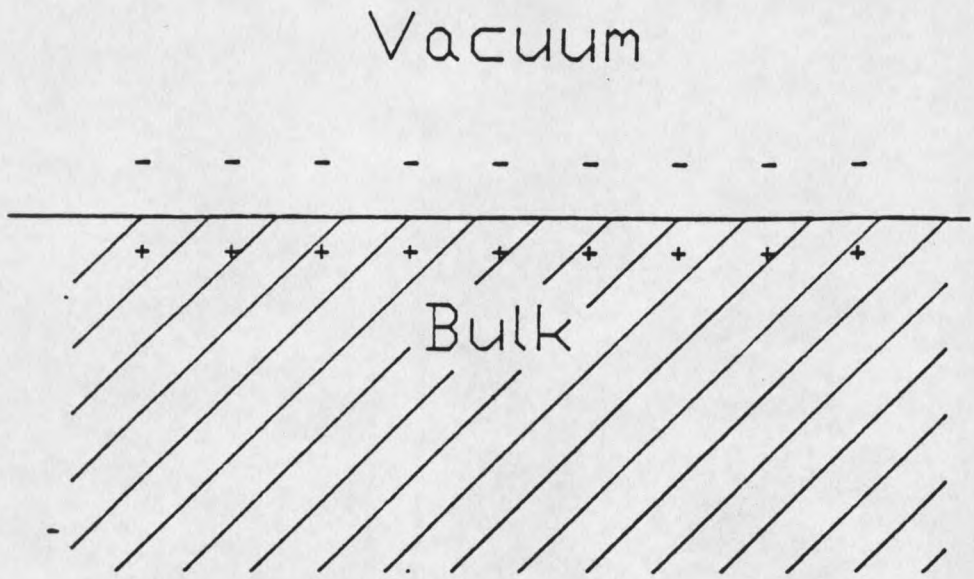

Figure 6: Double charge layer

Taking a derivative with respect to time of both sides of the previous equation yields

$$I = \frac{d}{dt}(CV_c)$$

I is the displacement current between the capacitor plates. When V_C is non-zero varying the distance between the plates will change the capacitance C and create a current. The capacitance for a parallel plate capacitor can be written as $C = \varepsilon_0 A/d$ where A is the area of the plates and d is the separation. If the distance d has the form $d = a\cos(\omega t) + d_0$, where ω is the frequency of oscillation and a is the amplitude of the vibration, the time derivative of the capacitance can be written as

$$\frac{dC}{dt} = -\frac{\varepsilon_o A}{(a\cos\omega t + d_o)^2} a\omega \sin\omega t$$

yielding a current of

$$I = -V_C \frac{\varepsilon_o A}{(a\cos\omega t + d_o)^2} a\omega \sin\omega t.$$

Inspection of this equation shows that if V_C is zero then the current is also equal to zero.

The Kelvin probe measurement can be described in terms of a simple capacitor circuit, c.f. Figure 7, in which the sample forms one side of the parallel plate capacitor and the probe forms the other. By adjusting the external potential the CPD can be nulled leading to zero current in the circuit. Use of a lock-in amplifier is customary because stray capacitances can lead to large currents not associated with the CPD between the sample and probe. A lock-in amplifier can be thought of as a high gain and high Q band pass filter. With the proper phase adjustment, the lock-in serves to isolate the current originating from the sample.

The work function change measurements were made in the 545 chamber described earlier. The Kelvin probe used for the measurements presented here was a molybdenum probe mounted on a piezoelectric crystal driven to oscillate at 170 Hz, the natural frequency of the assembly. Figure 8 gives a drawing taken from the operations manual of the Kelvin probe used for this experiment. The piezoelectric crystal on the probe was driven with a Kelvin control unit Delta-Phi Electronic Model 05. To measure a more stable current this control unit was modified so that an external lock-in amplifier, a Stanford Research Systems model SR510, could be used. The lock-in amplifier was interfaced using an ATT 6300+ computer for experimental control and data acquisition. The resulting system gave low noise and high sensitivity results and better performance over the lock-in integrated into the commercial Delta-Phi control unit.

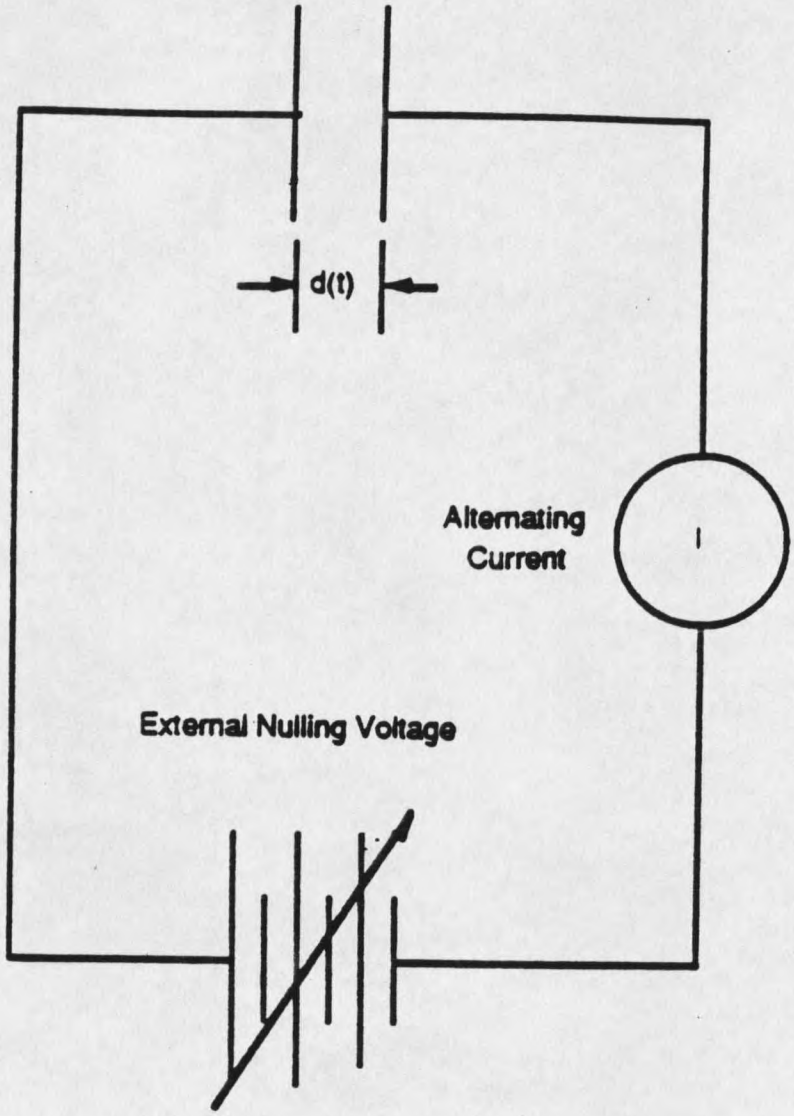

Figure 7: **Contact potential difference capacitor circuit**

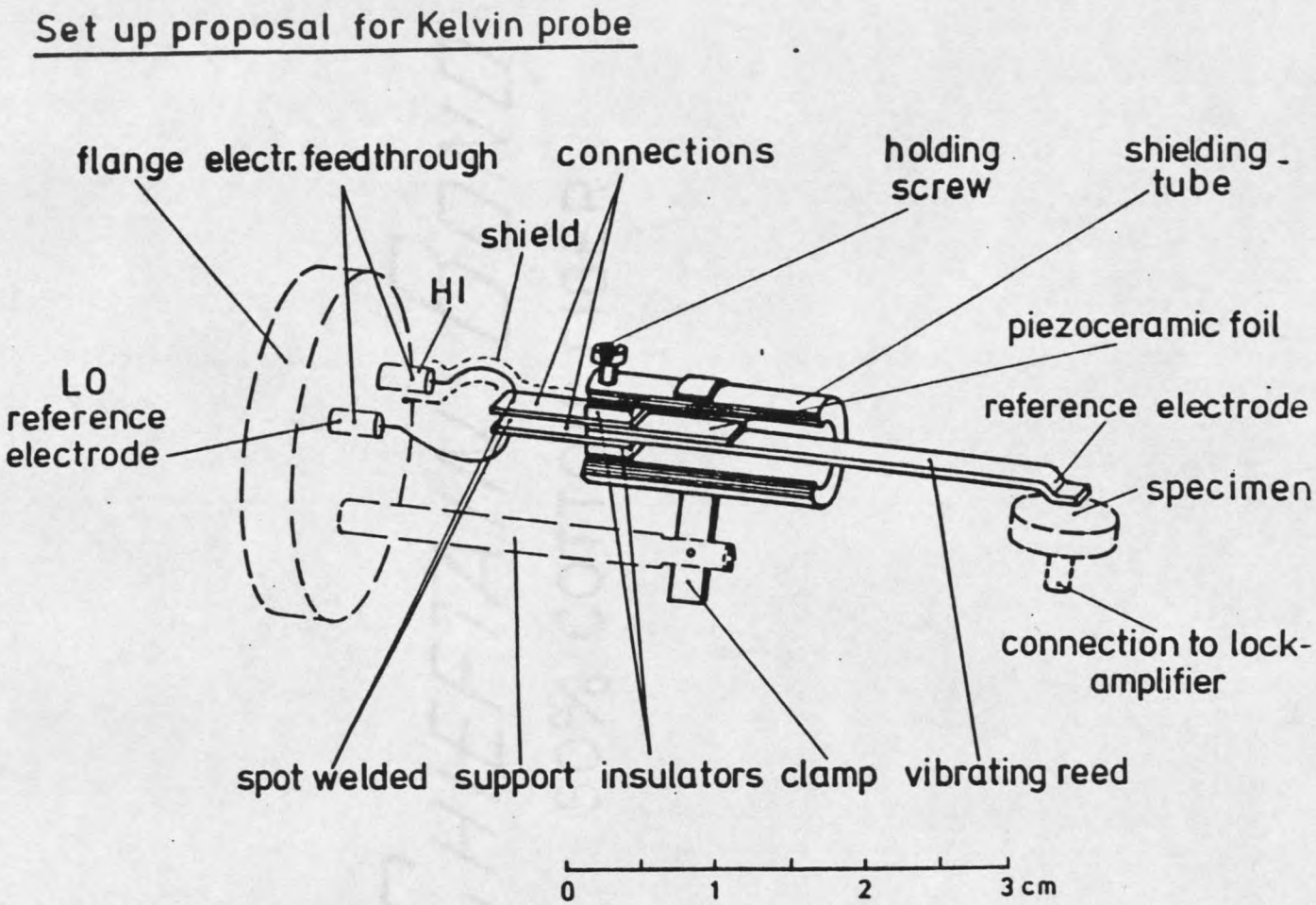

Figure 8: Drawing of Kelvin probe assembly

Surface Second Harmonic Generation

Laser generated second harmonic (SHG) radiation from materials has been used extensively since its first observation in the laboratory in 1961.[12] The theoretical development of SHG from the bulk was done as early as 1941 by Karplus and Schwinger.[13] The gap between the theoretical development and experimental observation occurred due to the fact that prior to the advent of the laser available light sources were not sufficiently intense for nonlinear optical processes to be observed easily.

Probing surfaces under UHV conditions with SHG is somewhat of a new development. SHG has surface sensitivity for systems having inversion symmetry within the bulk. It has been used to study the surface geometry of Si(111)[14] and to detect submonolayer molecular or atomic coverages on surfaces.[15] Unlike some surface science techniques SHG is nondestructive and allows real time measurements to be made during adsorption. Time resolved dynamics can be measured for which the time resolution is limited only by the repetition rate of the laser and, ultimately, the laser pulse width. Of the techniques discussed above the Kelvin Probe was the only technique that conveniently allows for nondestructive time resolved measurements of this type. The spatial resolution of SHG is limited only by the minimum spot size of the focussed laser beam. A spatial resolution of a micrometer has been achieved.[16]

In order to quantify the magnitude of the SHG signal for bulk systems Bloembergen and Pershan introduced nonlinear susceptibilities into Maxwell's equations.[17] Adapting Bloembergen and Pershan's approach, Chen et al.[18] have derived an expression for the intensity for the SHG beam upon reflection from a surface:

$$S = \frac{128\omega^4}{hc^3}\left|N_a\alpha^{(2)}\right|^2 I_1^2 AT \left(\frac{photons}{pulse}\right)$$

where N_a is the number of molecules per unit area, $\alpha^{(2)}$ is the nonlinear polarizability of the surface, I_1 is the intensity of the incident beam, A is the cross-sectional area of the beam, T is the pulse duration, and ω is the frequency of the incident light.

To understand the surface sensitive nature of this process better, the polarizability can be separated into two parts:

$$\alpha^{(2)} = \alpha_S^{(2)} + \alpha_A^{(2)}$$

where $\alpha_S^{(2)}$ and $\alpha_A^{(2)}$ are the nonlinear polarizabilities of the substrate and adsorbed atoms respectively. It is easy to see that the intensity of the SHG signal may change upon adsorption of atoms or molecules. One way for the intensity to increase is if $\alpha_A^{(2)} >> \alpha_S^{(2)}$. An example of this has been demonstrated by electrolytically depositing chlorine on silver.[18] Here the chlorine atoms formed highly ionic bonds with the substrate silver leading to significantly enhanced SHG from the surface. Alternatively, the adsorbate may induce changes in the electronic distribution and thereby changes in $\alpha_S^{(2)}$ which modifies the SHG signal. For example, Shen et al.[19] have shown how the SHG signal from Rh(110) decreases with the adsorption of O_2 and CO.

In our work the SHG measurements were made in the 545 chamber described earlier. Figure 9 shows a complete schematic of the optical setup. The laser used was a pulsed neodymium-doped yttrium aluminum garnet (Nd:YAG) Quanta-Ray model DCR-3. The fundamental wavelength of a Nd:YAG laser is 1.06 μ, the second harmonic of this being at 532 nm. The pulses were about 15 ns wide and the repetition rate was 10 Hz. Ten percent of the incident beam was reflected back through a quartz quarter wave plate to produce a second harmonic signal which served as a reference signal. Spectral filtering of the second harmonic light thus generated was accomplished using a BG-18 filter and an

interference filter. The reference signal was measured with a photomultiplier tube. Because the reference signal has the same dependence on laser fluctuations as the signal from the sample it was used to factor out the variations in laser power as the data was collected. This is important because small fluctuations in the fundamental are amplified quadratically in the SHG signal. After passing through the reflector the primary beam passed through a Fresnel rhomb to rotate the electric field polarization and then was directed into the experimental chamber. The beam entered the chamber through a standard Varian glass window attached to a 2.75" Conflat flange and was incident on the sample at an angle of 22.5°. A power density at the sample of 280 mJ/cm^2 was typically selected. The reflected beam exited the chamber through a similar glass window attached to a 6" Conflat flange. The spectral filtering was performed in the same manner as for the reference signal except a KG-3 filter was used instead of BG-18. The attenuation of these filters at 1.06 μm is approximately the same. Different filters were used because of availability.

An integrating boxcar was used to process the signals from the two photomultiplier tubes. This is standard practice when making measurements of a pulsed nature to increase signal to noise ratio. Figure 10 presents a schematic diagram of the electronics. Prior to entering the boxcar the signals were each delayed by 75 ns. This was necessary because after the boxcar is triggered there is about a 50 ns delay before it can start integrating. The trigger source was a photodiode that was placed along the path of the reference signal. The reference signal was presented to the boxcar without any amplification. The signal from the sample was amplified by a factor of ten prior to input to the boxcar. The average integrated signal from each channel A and B were digitized by two analog to digital converters contained in the SRS 510 lockin amplifier. The lockin was interfaced to an ATT 6300+ computer which would read the digitized signals and plot the ratio of the sample signal from A to the reference signal from B. Because the intensity

variation due to the laser is common to both signals plotting the ratio of the two signals serves to cancel out fluctuations in the laser intensity.

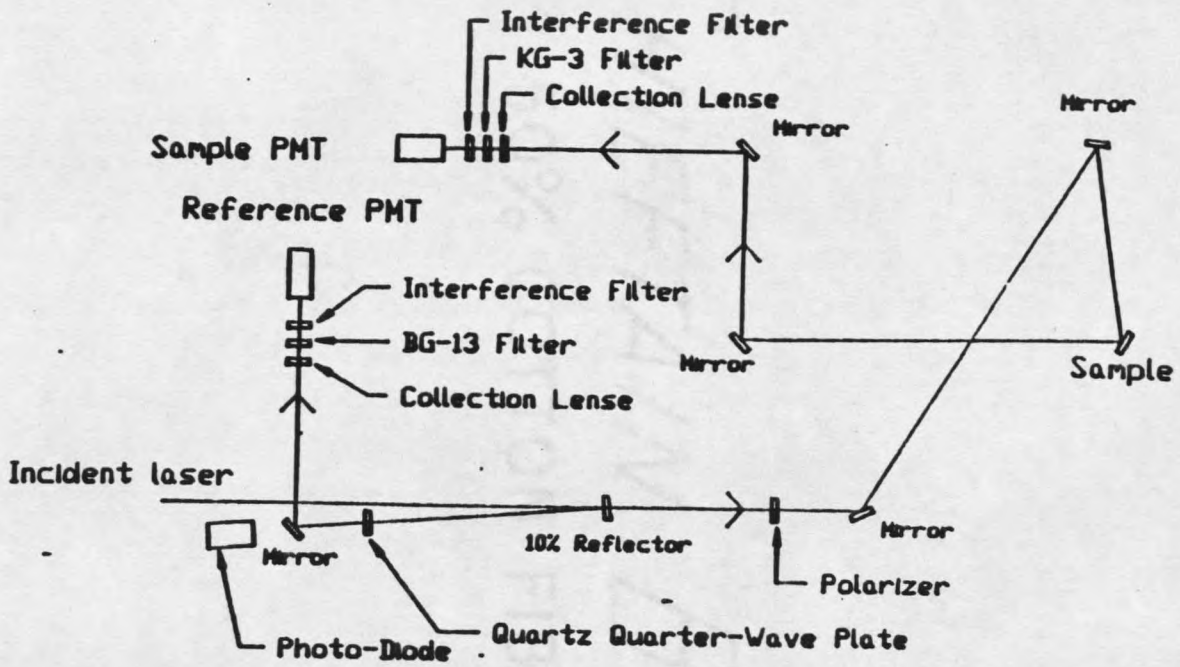

Figure 9: Optical setup for SHG experiment

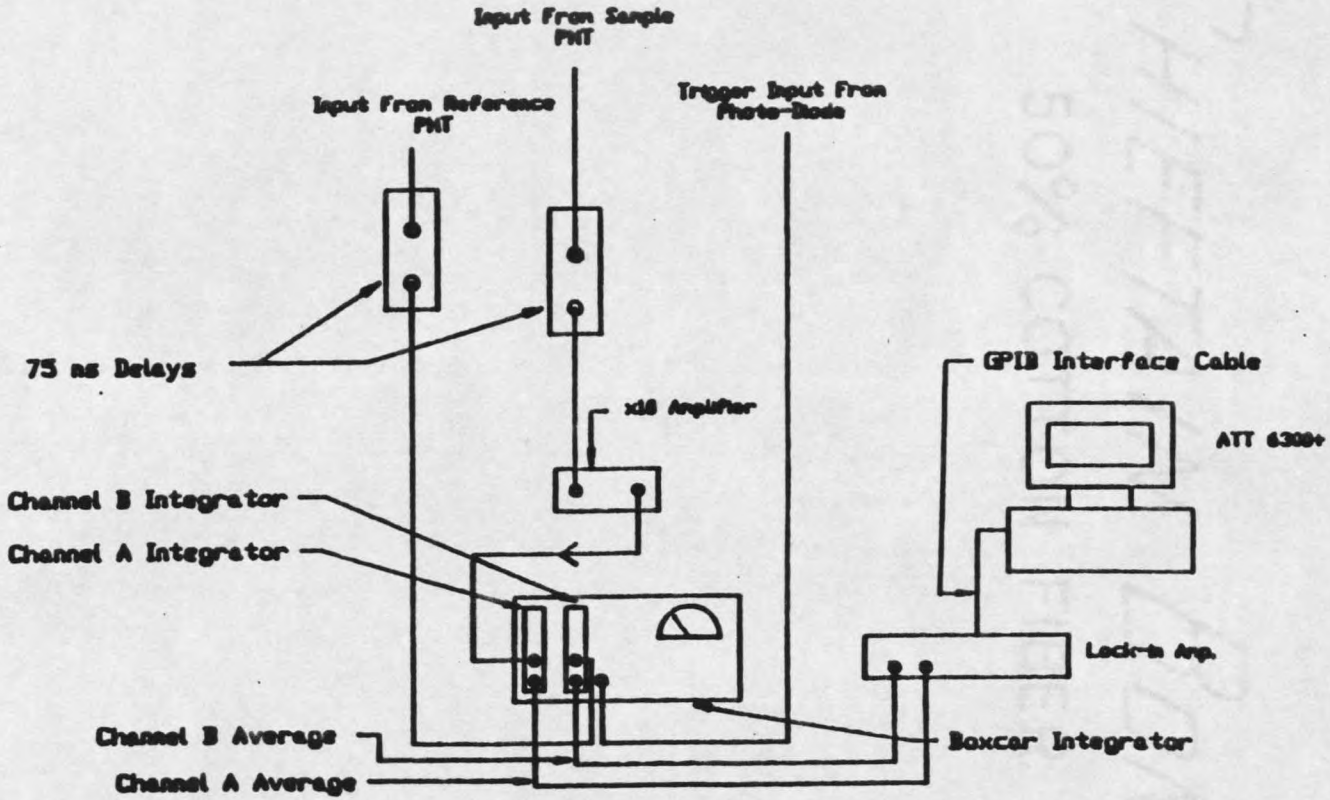

Figure 10: Electronics schematic for SHG experiment

CHAPTER 3

PREVIOUS OXIDATION STUDIES

Very little is known about the surface properties of nickel aluminum, in contrast to the case for nickel or aluminum. An interesting way to look at an alloy system is see if the alloy can be considered a "sum" of elements or as a new "element". Thus, to lay the ground work for discussing this perspective we present first a review of the extensive work done on the oxidation of elemental nickel and aluminum.

Oxidation of Aluminum

Aluminum is the most abundant metal in the earth's crust, comprising about 8.1% of the crust. Due to its favorable properties aluminum is widely used. These properties include low mass density, high thermal and electrical conductivities, high ductility and malleability, nontoxicity, and lack of magnetism. Possibly one of the most important properties is aluminum's ability to form rapidly a stable oxide on exposure to air that resists further corrosion. Aluminum has been applied in the manufacture of diverse items ranging from electrical transmission lines to artificial rubys for lasers.

The crystal structure of aluminum is face-centered cubic with a lattice constant of 4.05 Å. Figure 11 presents a view of the atomic arrangement of the three low index surface unit cells for a face centered cubic lattice. The (111) face is the one with the highest surface atomic density and the (110) has the lowest. The surface atomic densities are 0.86, 1.2, and 1.4×10^{15} atoms/cm^2 for the (110), (100) and (111) faces, respectively. The density of atoms on the surface is an important property of a system because it affects the number of

chemisorption sites available, the interatomic distances on the surface, and differences in work function between the faces.

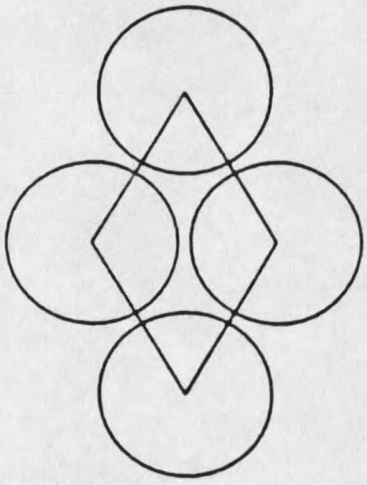

(111) Surface Unit Cell

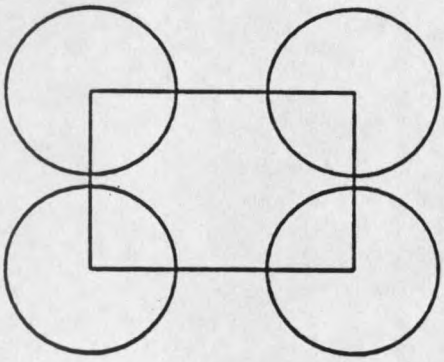

(110) Surface Unit Cell

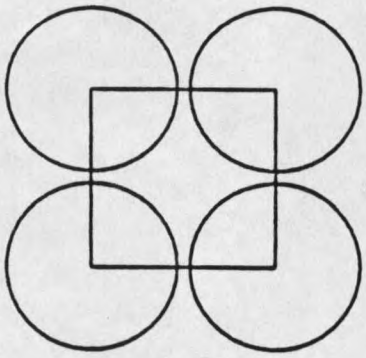

(100) Surface Unit Cell

Figure 11: Three low index faces for face centered cubic lattice

Oxygen is known to adsorb atomically on clean aluminum. Molecular adsorption has been observed only on a few clean metals, specifically platinum, silver, gallium, and gold,[20] but only at low temperatures. Molecular adsorption was reported[21] for Al(111) at 30 K but this adsorption probably occurred on a surface already contaminated with oxygen. By examining the comparative energies of dissociation for O_2 and AlO, it is readily seen that dissociation of O_2 is energetically preferred. The dissociation energy of O_2 is 5.115 eV and for AlO it is 5.15 eV. Thus when O_2 dissociates forming two AlO bonds, the gain in energy is about 5 eV.

Aluminum oxide formation has been extensively studied using XPS. The Al 2p core level has a binding energy that ranges from 72.65 eV for elemental aluminum and to 75.3 eV for Al_2O_3.[22] Core level shifts arise due to the change in electrostatic potential at the core level for different bonds and in different bonding configurations. In an experiment on polycrystalline aluminum Flodström et al. reported three different spectral lines observed in the Al 2p region as the sample was oxidized.[23] The incipient phase of oxidation was shown to produce an Al 2p peak to lie in position between the Al 2p peaks corresponding to elemental aluminum and those of Al_2O_3. The intermediate peak occurred at an oxygen exposure of 50 L* and had a binding energy 1.4 eV greater than the elemental Al 2p peak. At an exposure of 100L the third peak appeared at a binding energy 2.7 eV higher than the clean Al 2p. This third peak indicated the development of a fully oxidized aluminum species found in Al_2O_3. The explanation presented of the second peak was that at low exposures a chemically different Al-O bond is formed. Flodstrom et al. repeated this experiment for single crystal Al(111) and found the results were approximately the same as for the polycrystalline case.[23]

---

* L denotes the Langmuir unit of exposure: an exposure of 1×10^{-6} Torr for one second or approximately one monolayer of coverage if the sticking coefficient were unity.

Many conflicting results have been reported for the change in work function of aluminum with oxygen exposure. The conflicting results include: different magnitudes, shapes, and the amount of oxygen required to reach saturation. Presumably these experimental inconsistencies are due to different surface preparation techniques. For example, Bradshaw et al. showed the work function change measured was dependent on the sputter and annealing process.[24] Some of the techniques that have been used to measure the work function change on aluminum include: Fowler plots of photocurrent,[25] measurement of the changing width of the photoelectron energy-distribution curves,[26] and the Kelvin probe method.

To understand better how changes in work function can be used to infer the characteristics of the oxided aluminum surface, consider first the results for elemental aluminum. Work function measurements made on clean low index surfaces of aluminum have been performed by Eastment and Mee.[25] The values reported for the (111), (100), and (110) crystal faces were 4.26, 4.20, and 4.06 eV, respectively. These results are consistent with a simple physical argument first presented by Smoluchowski stating that the more open surfaces of nearly free electron metals should have lower work functions.[27] This argument is based on the following idea: electronic charge at any surface will tend to spill out into the vacuum lowering the electronic energy by delocalization. In addition, the electrons will tend to redistribute themselves within the surface region in order to reduce the curvature of the charge density contours, thereby, also reducing the energy of the system. The result of negative charge moving into the vacuum is the creation of a double charge layer whose dipole moment points toward the bulk. The more open the surface the greater the charge redistribution within the surface layer and the less charge moves into the vacuum. This provides a smaller surface dipole and a lower work function. Comparing the trend reported by Eastment and Mee to the surface atomic densities for these low index faces supports the veracity of this simple picture.

The same picture should also be useful to interpret work function changes in chemisorption systems such as oxygen on aluminum provided the substrate geometry is not significantly disturbed by the adsorbed species. That is, using this model changes in the equilibrium charge distribution due to the presence of adsorbates can be inferred from the the work function data and models of bond geometries can be proposed. Hofman et al. studied the dependence of work function versus oxygen exposure, for the (111), (110), and (100) crystal faces.[21] Figure 12 is a reproduction of their measurements, performed using a Kelvin probe. In all three cases the work function went down upon initial oxygen exposure. At high exposures the total work function change was largest for the (100) face and smallest for the (111) face. The curves were monotonic for both the (110) and (100) faces but not for the (111) face, which had a minimum at 50L and then rose to saturation at 200L. Adsorption kinetics were shown to be important in several respects. First, the positions of these extremas were found to be exposure rate dependent. Second, the change in work function for the (111) face was partially reversible when the oxygen source was interrupted. That is, after removing the oxygen source the work function would increase, the degree of which was also pressure dependent. When the sample was exposed at a pressure of $1x10^{-6}$ Torr the work function reversal would amount to about 80 meV. When the oxygen was removed at $5x10^{-8}$ Torr the increase was only about 20 meV. This reversibility was only exhibited in the (111) face.

The results of Hofman et al.[21] differ significantly from the results of Gartland[28] for the (111) surface. Although Gartland[28] used Fowler plots of the photoelectron current to measure the work function, both groups used the same sample preparation techniques. In the (110) and (100) cases the work function change versus exposure curves exhibited the same general shape, only differing in the total change. The total work function change as measured by Gartland[28] was about 150 meV, 80 meV, and 490 meV for the (110), (111), and (100) faces, respectively. For the (111) face the work function change measured by the two

groups was in total disagreement. Gartland[28] measured the change to be positive and Hofman et al.[21] negative. Michel et al.[29] reported results for work function changes with oxygen exposure that closely parallel the measurements made by Hofman et al.[21] However, Michel et al.[29] measured a greater total change in the work function and the saturation coverages were larger.

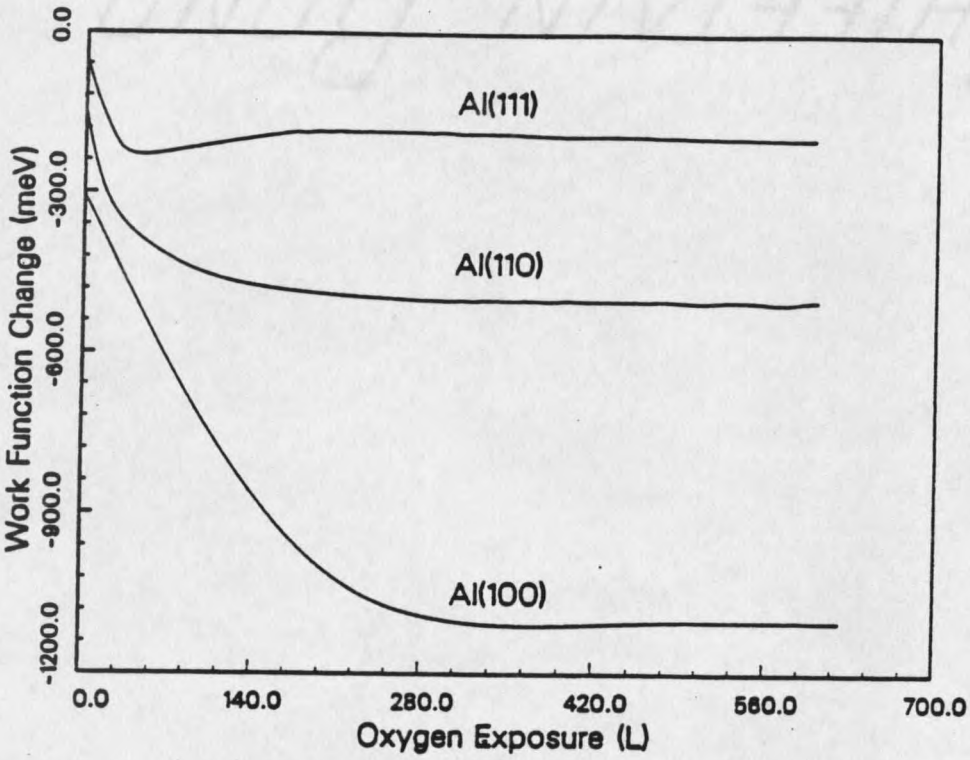

Figure 12: Work function change versus oxygen exposure for aluminum (100), (110) and (111) (reproduced from Ref. 21).

Auger electron spectroscopy has been used to access the atomic concentration of oxygen and formation of Al_2O_3 on elemental aluminum substrates. Elemental aluminum has two predominant Auger electron kinetic energy peaks, one at 68 eV and the other at 1396 eV. When oxygen interacts with aluminum forming alumina, ie. Al_2O_3, two additional peaks arise, one at 51 eV and the other at 1378 eV. The atomic concentration of

oxygen can be determined by examining peak height ratios between oxygen and aluminum. Formation of Al_2O_3 can be monitored by watching for the appearance and growth of peaks at 51 eV or 1378 eV.

Michel et al.[29] studied the initial oxygen aluminum interaction for the low index faces (111), (110), and (100) using Auger electron spectroscopy. In Figure 13 we reproduce their AES results for the uptake of oxygen. For each case three distinct phases were observed in the adsorption kinetics. The first phase was a rapid linear increase in the peak height for the oxygen peak at 510 eV. This was accompanied by a correspondingly rapid decrease in the peak height for the elemental aluminum line at 68 eV. At the beginning of the second phase the peak at 51 eV corresponding to oxidized aluminum was apparent and increased in a linear fashion until the end of the second phase. The third phase of adsorption curve was characterized by the three peak heights reaching saturation levels. The three different crystal faces had characteristic exposures for the start and finish of each phase. The first phase ended at exposures ranging from 20 L to 55 L. The second phase ended at exposures from 55 L to 120 L. The breaks at the first and second phase were attributed to completion of the first and second oxygen layers.

Erskine and Strong performed a high resolution electron energy loss spectroscopy study of the oxidation of Al(111).[30] At all exposures the spectra exhibited three loss peaks. The two primary peaks were at 80 meV and 105 meV, and the third peak was at 40 meV. The peak at 105 meV grew in relation to the peak at 80 meV as the exposure increased. After each of the exposures they heated the crystal to 500°K. This caused the peaks at 40 meV and 105 meV to grow. They attributed the peak at 105 meV to subsurface oxygen, the peak at 80 meV to surface oxygen, and the peak at 40 meV to a coupled mode between the surface and subsurface modes. Later this group performed a theoretical investigation of this system using a lattice dynamical model.[31] Their findings were in agreement with their experimental results. The important conclusion of these two investigations is that at all

exposures both surface and subsurface adsorption exist . This conclusion seems to contradict the picture developed by previous workers for this system.

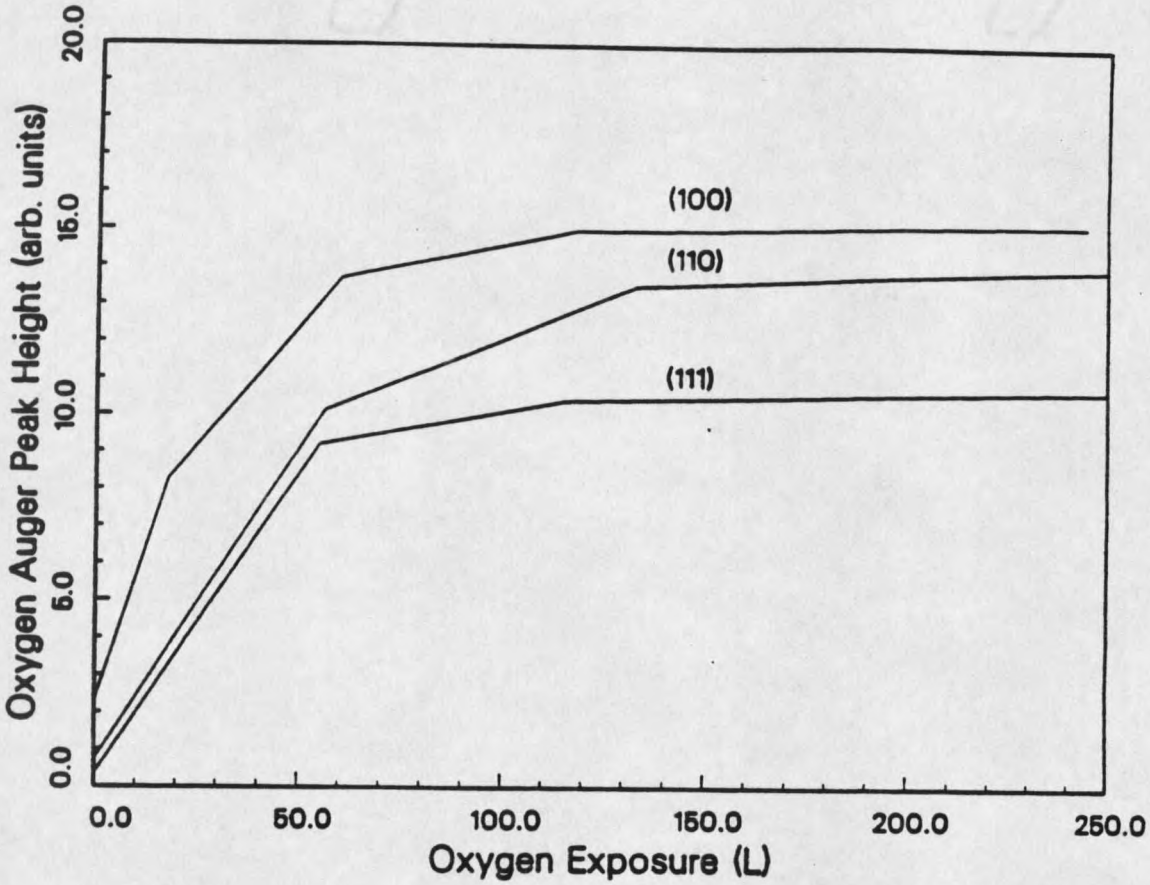

Figure 13: AES oxygen uptake for aluminum (100), (110), and (111) (reproduced from Ref. 29)

Oxidation of Nickel

Like aluminum, bulk nickel is a face centered cubic structure. With a lattice constant of 3.52 Å, the surface atomic densities for nickel are 1.14, 1.59 and 1.85 x 10^{15} atoms/cm^2 for the (110), (100) and (111) faces, respectively. Nickel has a reasonably high malleability and ductility, moderate thermal and electrical conductivities, and has a

room temperature ferromagnetic phase. Nickel is used extensively in alloys, most notably in stainless steel and other corrosion resistant alloys.

Elemental nickel has XPS peaks at binding energies of 873 eV ($2p_{1/2}$), 853 eV ($2p_{3/2}$), 112 eV (3s), and 69 eV ($3p_{1/2}$).[22] When oxygen interacts with nickel and forms NiO the separation between the spin orbit split $3p_{1/2}$ and $3p_{3/2}$ increases from 17.4 eV to 18.4 eV. In addition, a higher binding energy satellite associated with each of the $3p_{1/2}$ and 3p3/2 levels to indicate oxide formation.

Norton et al. performed an XPS study on the interaction of oxygen with the three low index faces of nickel.[32] On the clean nickel faces, the Ni $2p_{3/2}$ core level was at a binding energy of 852.8 eV and had a satellite at 858.6 eV. When the crystals had a heavy oxide this peak shifted to 855.1 eV and the satellite shifted to 861.8 eV. The O 1s peak binding energy was fixed at 529.7 eV for all exposures for the (111) face. However, the full width at half maximum changed from 2.0 to 1.8 eV over a coverage range from 0.3 to 3.0 monolayers. At high oxygen coverages the other two faces had the same O 1s characteristics as observed for the (111) surface. However, at coverages less than 0.3 monolayers the binding energy of the O 1s on Ni(110) and Ni(100) changed rapidly from 530.4 eV to 530.2 eV.

Demuth and Rhodin[33] carried out a chemisorption study on the three low index faces of nickel, utilizing work function measurements , LEED intensity versus voltage curves, and AES. For the (100) and the (110) surfaces they used a Kelvin probe for the measurements and for the (111) case the retarding field method was used. The work function in all three cases increased up to an oxygen coverage of one half monolayer and then decreased. The initial increase was largest for the (111) surface and smallest for the (100) surface. Holloway and Hudson[34] performed similar measurements on the (100) surface of nickel. Their results closely resemble the results of Demuth and Rhodin.[33] In Figure 14, a reproduction of Holloway and Hudson's[34] results for the (100) face, the work function change is plotted against oxygen Auger peak height, which is thought to be simply

related to the surface coverage. Finally, Evans et al.[35] also reported work function measurements on the three low index faces. The shape of the work function versus oxygen coverage curves were similar to those measured by the other two groups and no discernible differences were found in the total work function change for three different faces.

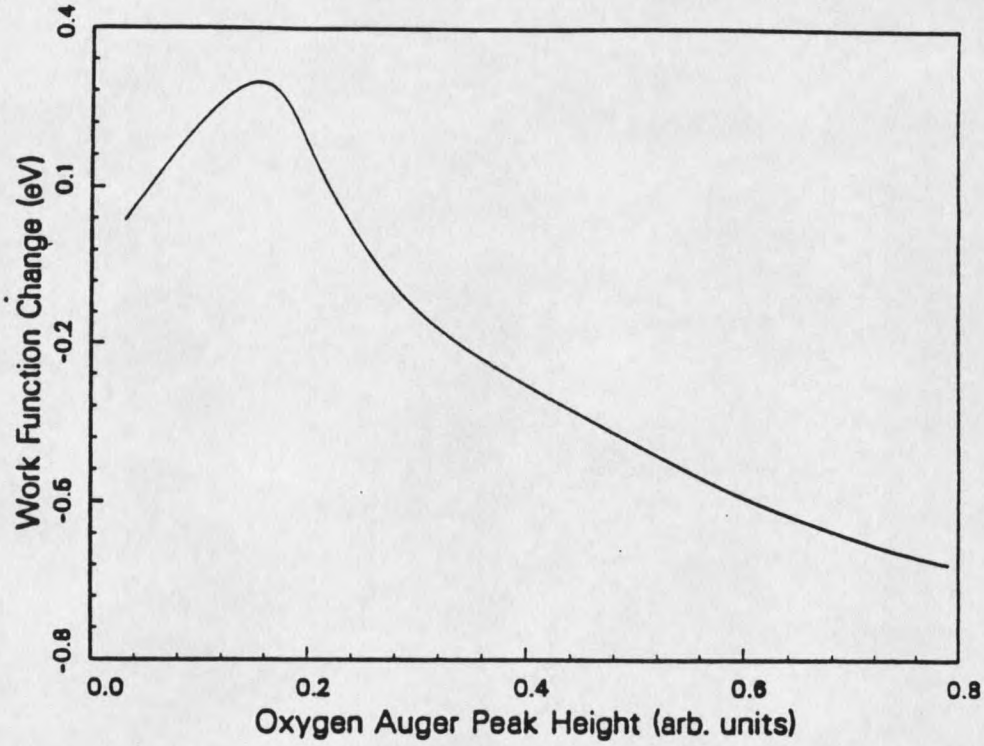

Figure 14: Work function change versus exposure for Ni(100) (reproduced from reference 34)

Nickel has predominant Auger peaks at 61 eV and 848 eV.[36] There is not any significant shifting of the nickel peaks as an oxide is grown on the surface. Therefore, the formation of NiO cannot be directly determined from the Auger energy position spectra, although line shape analysis might be employed. The rate of oxygen adsorption can be measured by plotting the Auger peak heights as a function of exposure. From this information coupled with other measurements the kinetics of NiO growth can be determined.

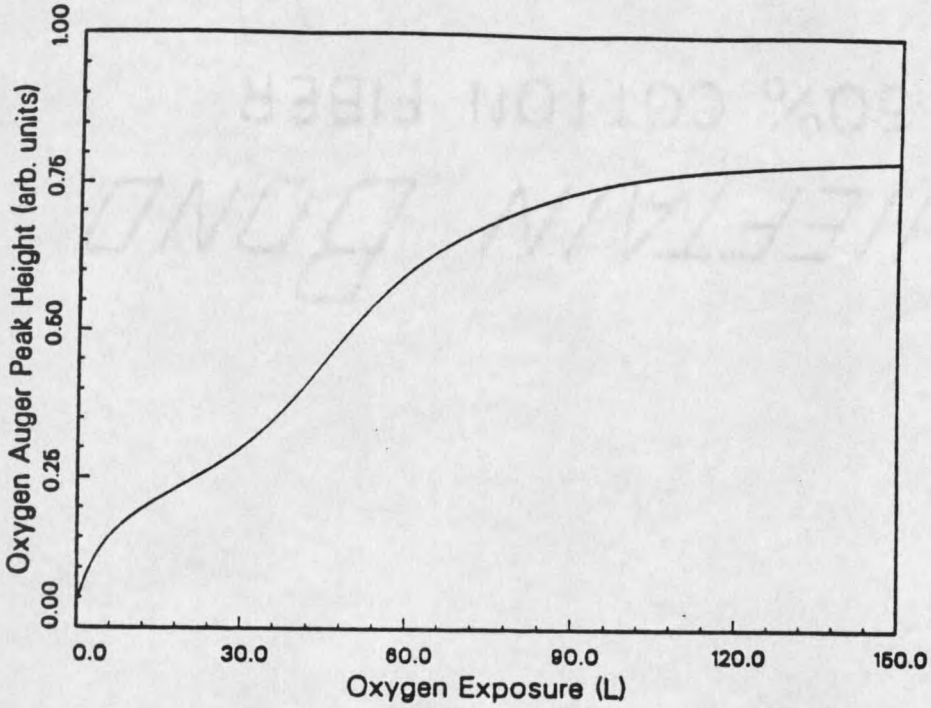

Figure 15: Oxygen uptake for Ni(111) (reproduced from reference 34)

Holloway and Hudson[34] utilized AES in a study of oxidation kinetics for the nickel (111) and (100) surfaces. Figure 15 and Figure 16 display their results for the (111) and the (100) faces, respectively. The curves describing the uptake for both surfaces had similar four phase shapes. The first phase is characterized by a rapid uptake. This phase is completed by exposures of 2.5 L and 1 L for the (111) and the (100) surfaces, respectively. During the second phase the adsorption rate slows significantly and then increases during the third phase. Saturation is attained, during the fourth phase at about 170 L for the (100) face and about 47 L for the (111) face. Combining these measurements with their LEED measurements they were able to draw the following conclusions. The first phase of exposure corresponds to chemisorption of oxygen which forms a surface structure with the same periodicity as the substrate. Formation of NiO occurs during the second phase and thickens during the third phase.

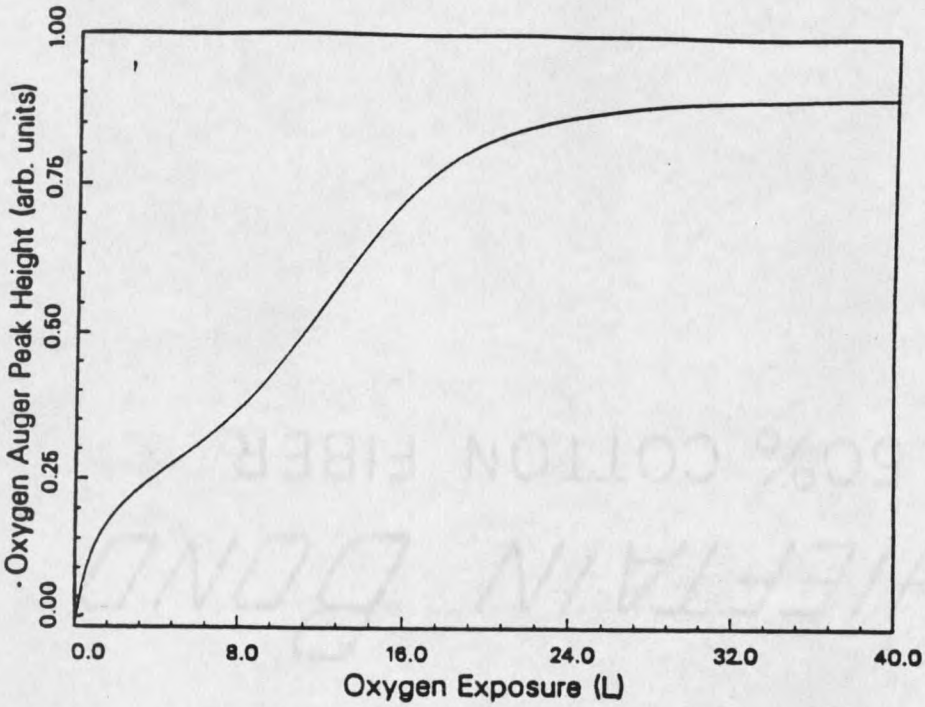

Figure 16: Oxygen uptake for Ni(100) (reproduced from reference 34)

Oxidation of Nickel Aluminum

Two groups have investigated the oxidation of nickel aluminum. Zehner and Gruzalski[37] studied the oxidation of all three low index faces using both AES and XPS. All three faces exhibited similar oxidation patterns, differing only in initial sticking coefficients. They calculated the initial sticking coefficient for the (110) and (111) faces and found the coefficient for the (111) face to be about 20 times higher than that of the (110) face. Although, they did not calculate the sticking coefficient for the (100) face they felt it is close to the value found for the (111) case. Analysis of their XPS data showed for all three faces a strong interaction between the adsorbed oxygen and the aluminum, and little or no interaction between the oxygen and the nickel. At 3000 L and higher exposures an additional peak formed at a binding energy 2 eV higher than the Al 2p peak on the (110)

surface. The only change in the nickel core level spectra was a gradual attenuation in the signal, implying little chemical interaction between the oxygen and the nickel.

Lui, Plummer, and Zehner[38] performed a photoemission study of the (111) face of NiAl using synchrotron radiation. Their results correspond to Zehner and Gruzalski's[37] regarding the formation of an aluminum oxide. Using synchrotron radiation they were able to do photoemission studies that were extremely surface sensitive by choosing appropriate photon energies. After exposing the surface to 2 L of oxygen an additional peak formed at a binding energy 1.8 eV higher than the Al 2p peak. Although, they only studied the (111) surface, it is assumed that all three faces form an aluminium oxide at lower coverages than reported by Zehner and Gruzalski[37]. The conclusions of both of these studies is that an aluminum oxide is being formed on all three low index faces. Combining these two investigations, Zehner and Gruzalski[37] concluded that aluminum is diffusing out upon exposure to oxygen.

CHAPTER 4

EXPERIMENTAL RESULTS FOR NICKEL ALUMINUM

Nickel aluminum has a cesium chloride crystal structure, described as a body-centered cubic having a two atom basis. An alternative description of the cesium chloride structure, is two interlocking simple cubic lattices. Each atom in the crystal has four nearest neighbors of the opposite type. The lattice constant of this system is 2.89 Å and the nearest neighbor distance is 2.50 Å.[39] The bulk truncated (110) surface from this structure consists of composite layers containing equal amounts of aluminum and nickel. Figure 17 displays a top view of the surface.

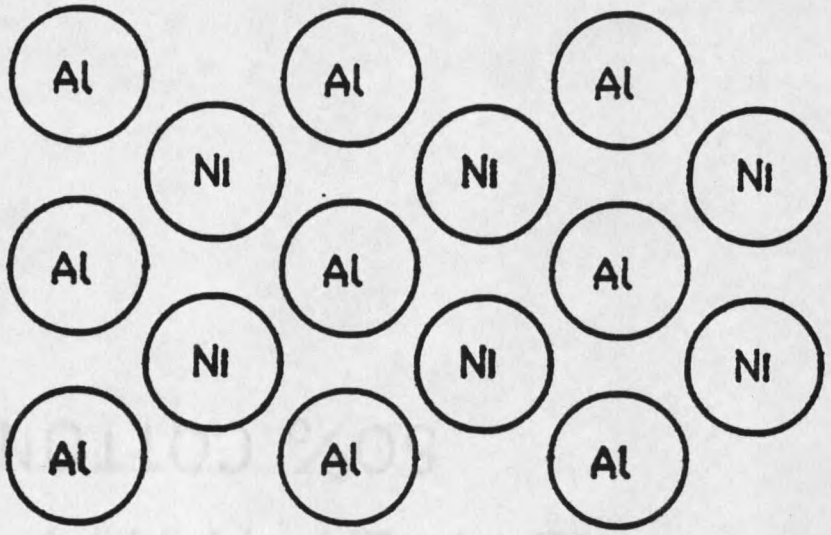

Figure 17: Top view of the NiAl(110) surface

Noonan and Davis have shown by analysis of LEED intensity versus voltage curves that the (110) surface exhibits rippled relaxation in the first plane.[40] The aluminum atoms on the surface plane relax outward 0.13 Å or 4.6% of their bulk spacing and the nickel atoms relaxed inward 0.17 Å or 6.0%. More recently Yalisove and Graham[41] showed that the (110) surface has a multilayer rippled structure. They studied the structure of the surface region with medium energy ion scattering and found that the first layer relaxes in the same fashion as proposed by Davis and Noonan,[40] the only difference in the two results being the magnitude of the relaxation. Yalisove and Graham[41] found the displacements to be 5.0% or 0.14 Å, for the aluminum atoms and -7.0%, or 0.20 Å, for the nickel atoms. In the second layer they found that the aluminum atoms relaxed inward 1%,or 0.03 Å, and the nickel atoms relaxed outward 1% of the bulk lattice constant. Figure 18 is a representation of the two layer rippled relaxation.

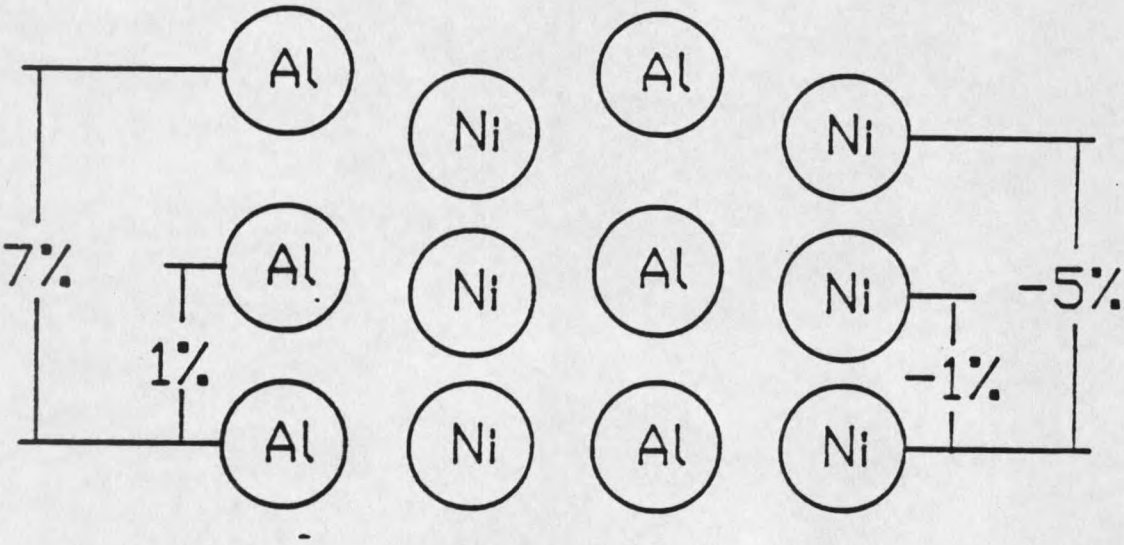

Figure 18: Proposed two layered rippled surface for NiAl(110)

Figure 19 shows representative spectra from the PHI 595 for both a clean (lower panel) and an oxided (upper panel) NiAl(110) surface. The analyzer on the 595 system is operated in the N(E) mode and the spectra plotted are dN(E)/dE. The differentiation is performed numerically, as opposed to most systems where a sinusoidal modulation voltage is applied to the analyzer. As discussed earlier the formation of an oxide on aluminum will cause two additional peaks to occur in the Auger spectra. These additional peaks will occur at 1378 eV and 51 eV. Examining the spectra in Figure 19 no apparent additional peaks occur due to oxygen exposure. Because the sampling depth of the 1378 eV electrons is around 12Å these electrons are not as sensitive to changes in the surface region as the low kinetic energy electrons. On the other hand the overlap of the low energy nickel and aluminum peaks near 60 eV makes it difficult to resolve the aluminum oxide peak at 51 eV. Finally, note that a carbon signal appears near 280 eV on the oxided surface. This is a common occurrence with NiAl(110) and occurred in each experimental chamber. Thus, we feel that carbon appears as a result of some sort of coadsorption process and does not arise because of impurities in the oxygen gas or crystalline bulk.

Figure 20 presents normalized Auger peak heights for the O KLL, Ni LVV, and the Al KLL peaks as a function of oxygen exposure. It is necessary to normalize the peak heights to factor out any instrumental differences from the spectra, the main ones being beam current and the multiplier voltage. The exposures were made at a pressure of 1×10^{-6} Torr in the PHI 595 UHV chamber. Denoting the Auger peak height of the ith element by P_i, the normalized peaks heights, P_A^{norm}, is computed using the following formula.

$$P_A^{norm} = \frac{P_A}{\sum_i P_i}$$

The uptake of oxygen is shown to be relatively smooth for all three curves with the rate of change of the peak heights for all three curves changing at about 1500 L. Of the three curves the oxygen shows the fastest rate of change for the first stage of the adsorption, followed by the aluminum, and then by the nickel. After 1500L the nickel peak height curve is flat, indicating no further decrease in the nickel concentration. During this stage the oxygen peak heights are increasing at a slow rate and the aluminum is decreasing at the same rate. Therefore, after 1500L the oxygen is behaving in a manner which does not affect the

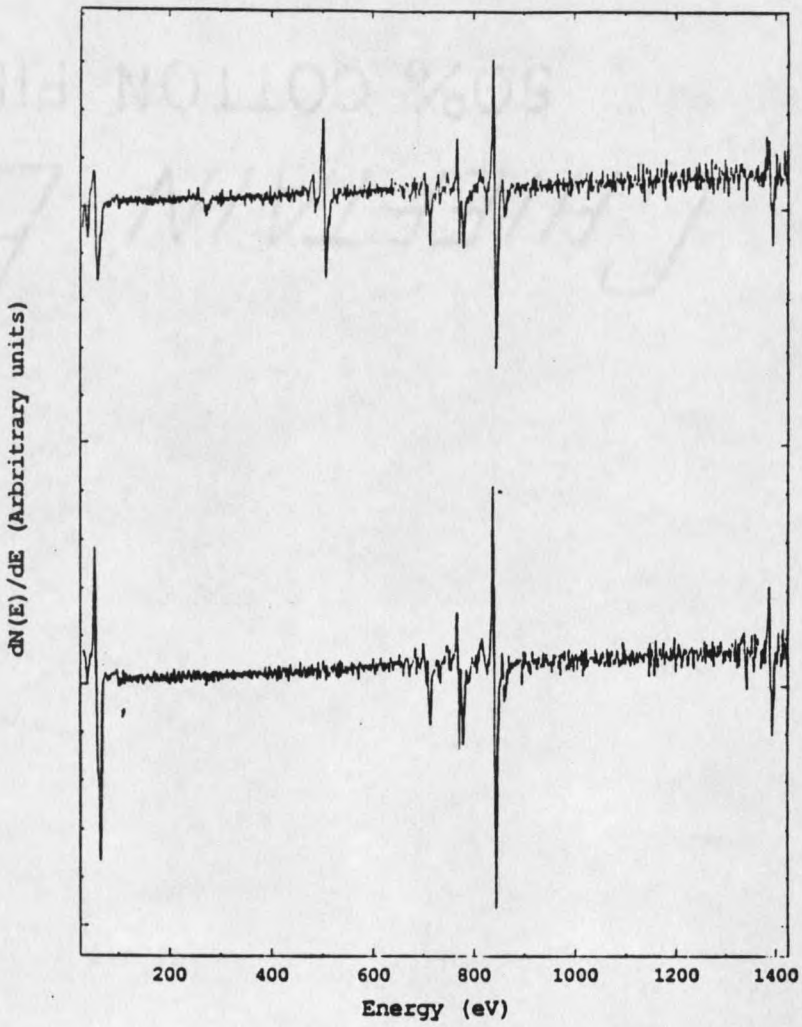

Figure 19: Representative Auger spectra from PHI 595

nickel concentration but only that of the aluminum.

Figure 21 shows the low energy nickel and aluminum Auger spectra for oxygen exposures up to 7000 L. The pressure during the exposures was 1 x 10^{-6} Torr and the exposures were carried out with the sample at room temperature. The 61 eV nickel peak and the 68 eV aluminum Auger peaks evolve with increasing oxygen exposure. Auger electrons in this energy range have the shortest mean free path and, therefore, come from the top-most layer. For example, electrons with an energy of 70 eV have a sampling of

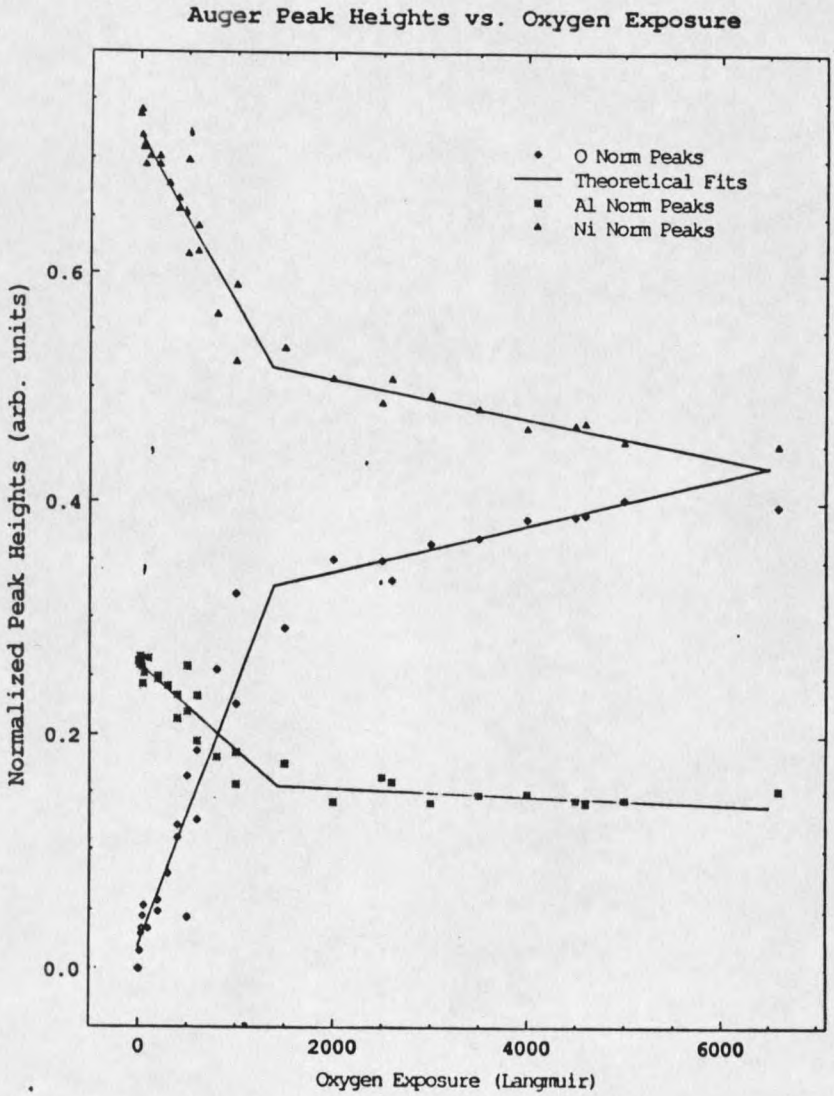

Figure 20: Normalized Auger peak heights versus O_2 exposure for NiAl(110)

around 2Å. In the Figure, line shape changes occur upon initial exposure and continue up to an exposure of 1500L. Further uptake of oxygen beyond approximately 1500 L does not seem to change the composition of the surface region as judged by AES. This set of oxygen uptake data was taken in the modified PHI 545 chamber. As with the data taken in the PHI 595 it is not possible to resolve an additional peak at 51 eV corresponding to Al_2O_3, because of the overlap of the aluminum and nickel peaks.

One other noticeable feature of Figure 21 is that the aluminum peak attenuates at a faster rate than the nickel peak. At an exposure of 700 L the two peaks have the same amplitude and can be clearly resolved. Further exposure causes the aluminum peak to decrease to an amplitude less than the nickel peak. The high energy nickel peaks near 800 eV showed only gradual attenuation with oxygen exposures greater than 1500 L but no concomitant changes in line shape. The sampling depth at 800 eV kinetic energy is significantly greater than that for electrons at 60 eV making the Auger spectra more indicative of changes in the deep surface/bulk region.

Figures 22 and 23 show two different results obtained for the change in work function versus exposure for the NiAl(110). Shown with the work function graphs are the Auger spectra obtained prior to the measurement, indicating the level of surface contamination before the exposure started. In Figure 22 there is little initial contamination due to oxygen and no detectable carbon signal. The Auger KLL line for carbon is at 280 eV and for oxygen is at 508 eV. In Figure 23, there are detectable amounts of carbon and oxygen prior to the oxygen exposure. The different amounts of contamination lead to two different work function changes, particularly in at beginning of the exposures. In the case of the clean surface, Figure 22, the initial action is a rapid increase in work function in which the work function increases by 50 meV over the first 30 L of oxygen exposure. For the slightly contaminated surface, Figure 23, there was no initial increase. However, after the initial exposure the change in work function for both cases is very

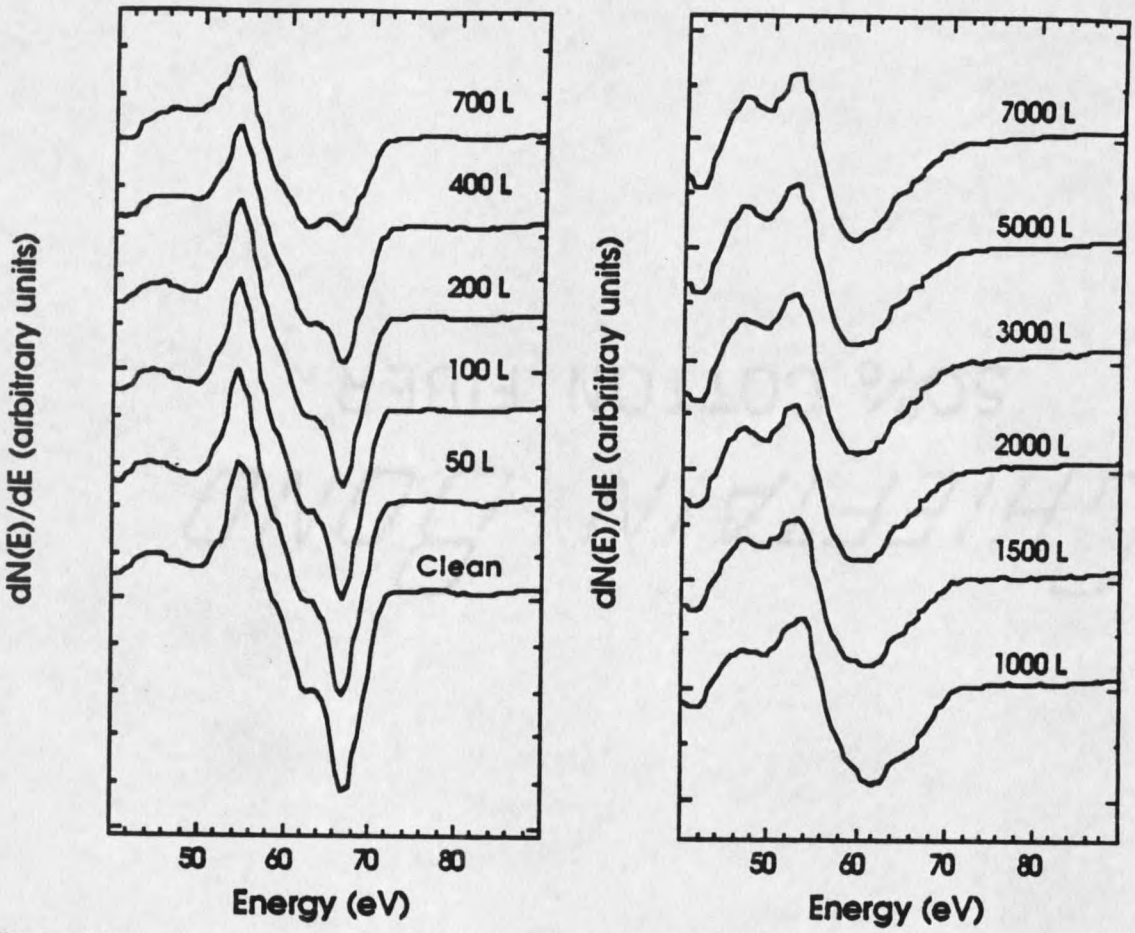

Figure 21: Low energy aluminum and nickel Auger peaks versus exposure

similar. The work function dependance on initial surface condition was a reproducible feature.

Another feature common to both Kelvin probe studies in Figure 22 and 23 is that when the oxygen is removed the work function decreases. This is a manifestation of the adsorption kinetics. The decrease is approximately the same for each case, falling immediately by approximately 25 meV over the first 25 L. The decrease is followed by a gradual increase back to the saturation value over approximately 2000 L. The work function decrease is more abrupt in Figure 22 than in Figure 23.

Figure 24 shows a typical result from the SHG intensity versus oxygen exposure measurement. The SHG signal stopped changing by an exposure of around 1200L. Within the limitations of the noise in the SHG system, there was no initial feature in the SHG that corresponded to the initial rise in the work function upon oxygen exposure. The SHG seems to gradually role off and plummet to its saturation value, approximately 80 % of the initial SHG signal level. Furthermore, as with the Kelvin probe measurements we removed the oxygen while measuring the SHG intensity. However, unlike the case for the Kelvin probe measurement, interrupting the oxygen source had no noticeable effect on the SHG signal level.

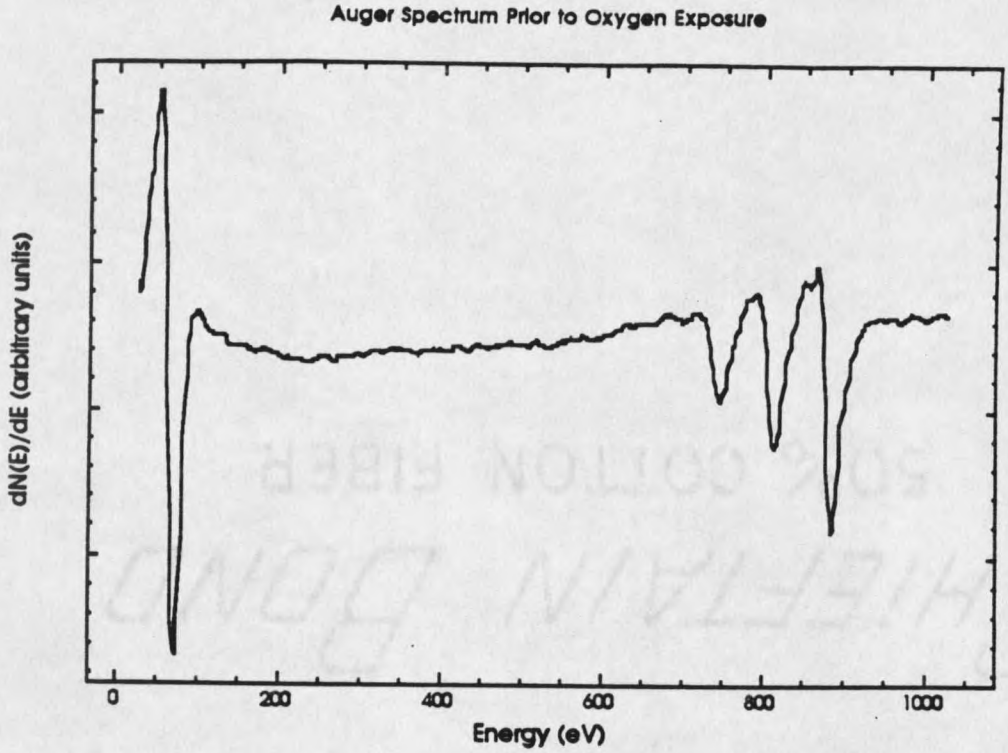

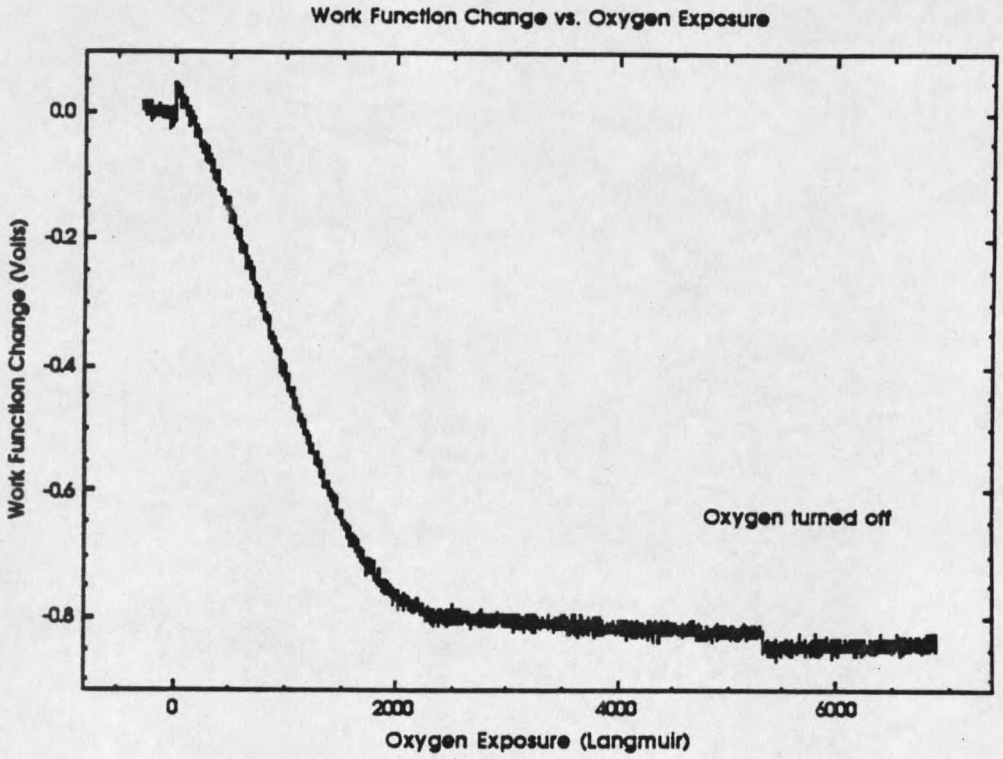

Figure 22: Work function change versus exposure for clean NiAl(110) surface

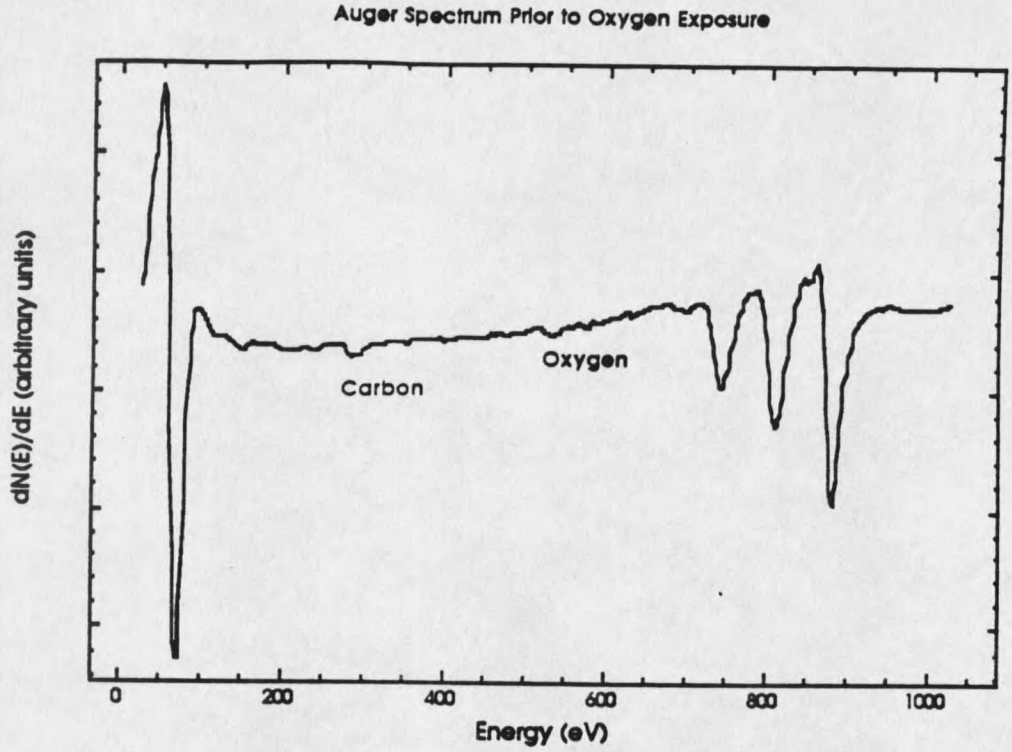

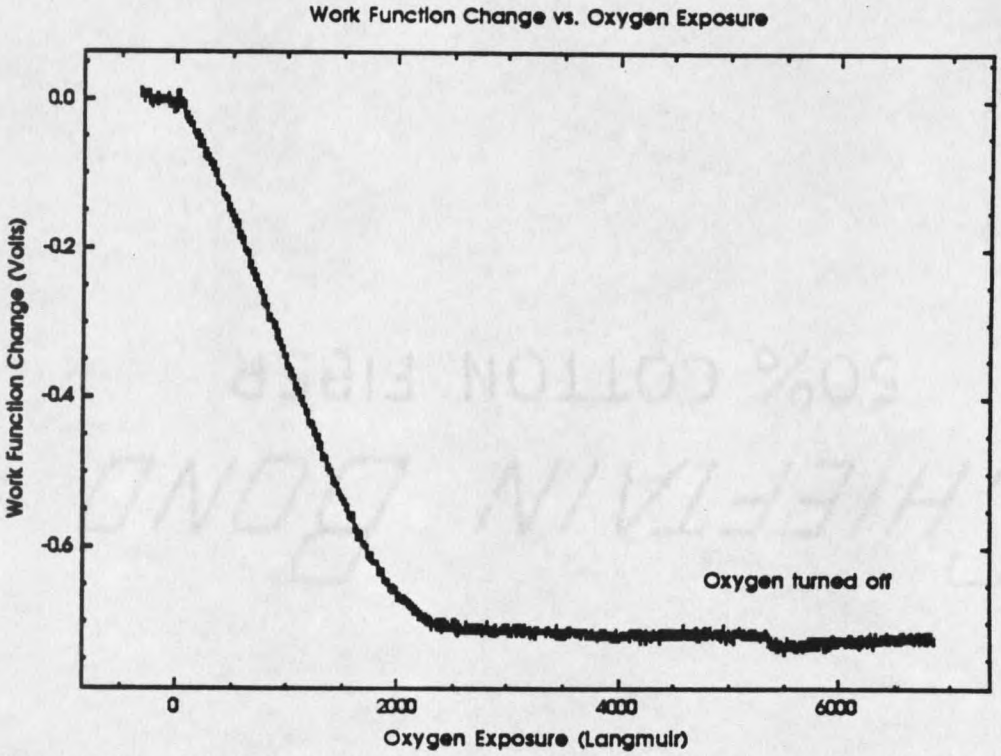

Figure 23: Work function change versus exposure for a contaminated NiAl(110) surface

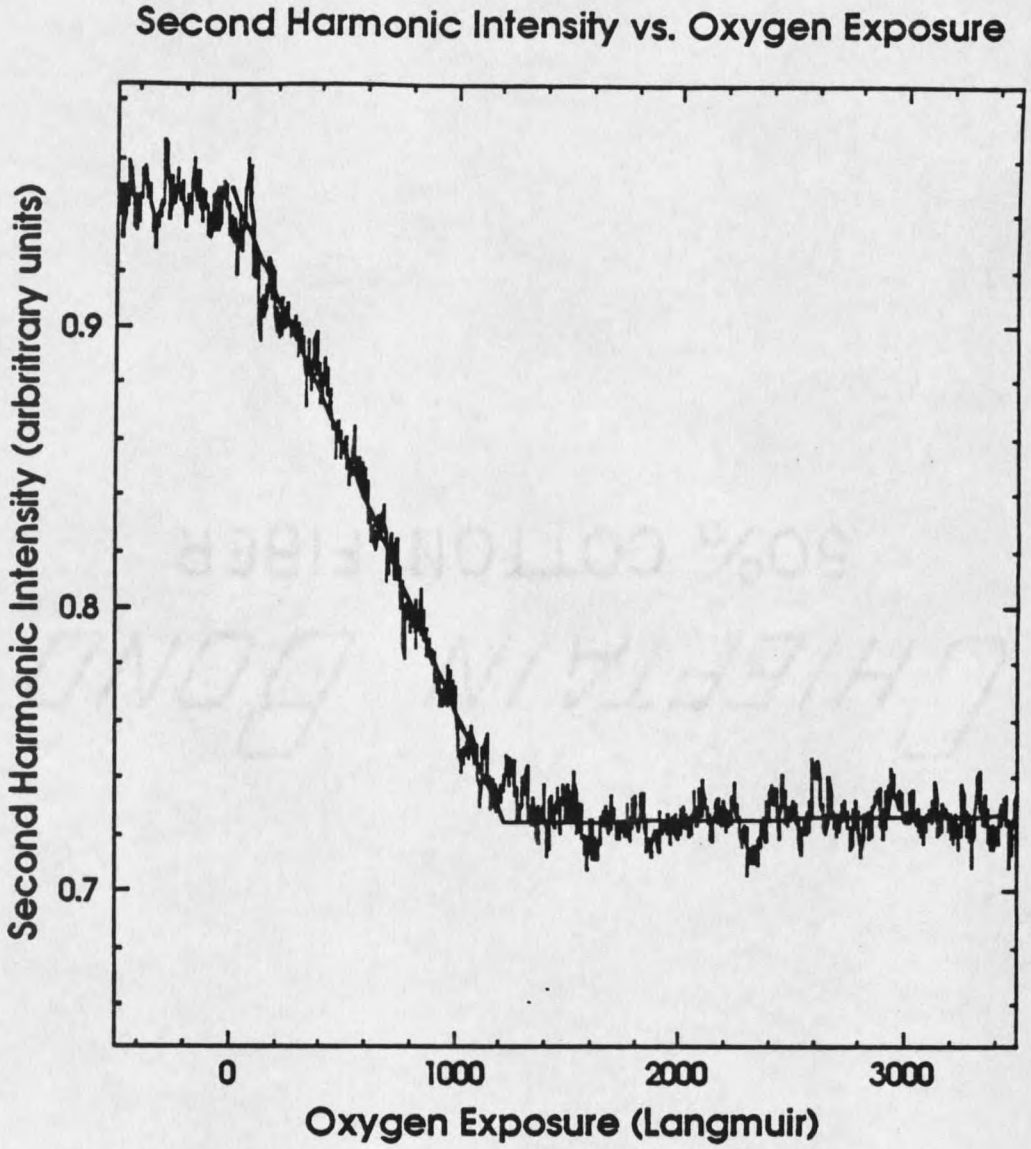

Figure 24: Second harmonic intensity versus exposure

Figure 25 shows the results of the XPS measurements for the Ni $2p_{1/2}$ and Ni $2p_{3/2}$ core levels for oxygen exposures up to 11000 L. The only noticeable change in the spectra as a function of exposure is a gradual decrease in the peak height of each peak with increasing exposure. Figure 26 is a plot of the Al 2p and Ni 3p XPS peaks for the same exposures as the previous figure. By an exposure of 7000 L an additional peak has formed at a binding energy about 2 eV greater than the Al 2p peak. At 11000 L the amplitude of this peak increases. In an effort to change the nature of the oxide on the oxygen saturated

surface we annealed the sample very rapidly, bringing the temperature up to 800 C in less than five minutes and then immediately removed the heat. The XPS spectra taken after the sample had cooled below 100 C showed no discernible changes in the Al 2p core level structure. Therefore, we feel no change in the oxide occurred due to this heat treatment, indicating that at saturation the oxide is stable.

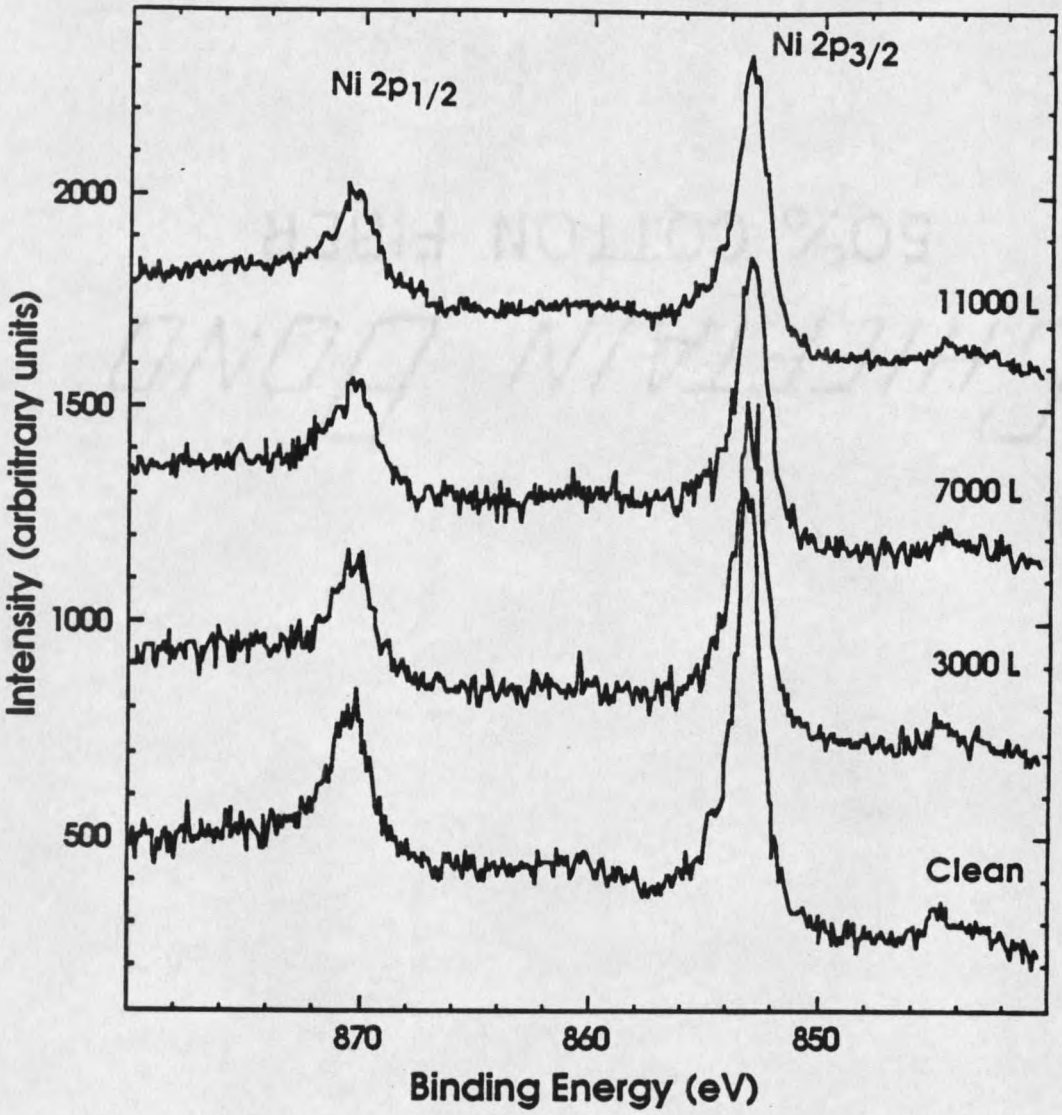

Figure 25: XPS spectra for Ni 2p core levels versus oxygen exposure

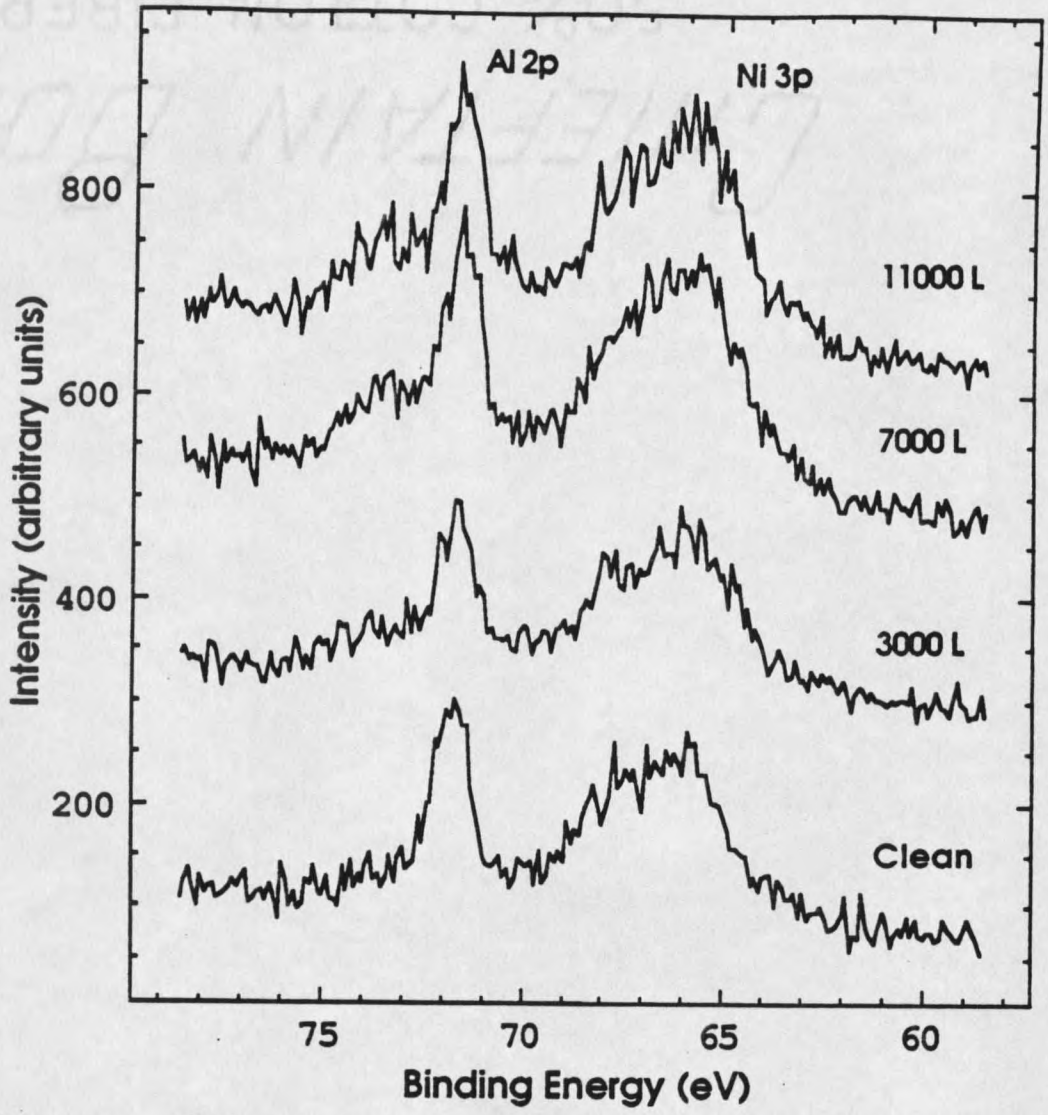

Figure 26: XPS spectra for Al 2p and Ni 3p core levels versus exposure

CHAPTER 5

DISCUSSION OF RESULTS

We have found that oxygen is weakly incorporated on the NiAl(110) surface. The oxygen that is adsorbed interacts exclusively with the aluminum in the substrate forming an aluminum oxide, although the oxide formed is probably geometrically or chemically different than Al_2O_3. There is little or no direct interaction between the nickel in the substrate and the adsorbed oxygen. However, the nickle indirectly affects the sticking coefficient by weakening the incorporation of oxygen into the surface. We feel the first stage of adsorption begins at the surface and is followed by subsurface incorporation. The oxygen is bound weakly enough that the oxygen on the surface is desorbed when the exposure stops and a diffusion process causes the oxygen from the bulk to migrate to the surface region.

First we will look at the the structure or characteristics of the oxygen saturated surface. The saturation point for the NiAl(110) surface we feel is at 1500 L ± 300 L. This is supported by SHG, Auger, and the work function measurements. First we will examine how the SHG intensity support this estimate. Referring to the plot of SH intensity versus exposure, Figure 24, the data can be fit well with two straight lines as presented on the Figure. These lines meet at an exposure of 1220L, implying the SHG intensity reaches a saturation level at a value somewhat greater than this exposure. The Auger data in Figure 21 shows that the line shape for the Al-Ni region stops changing in the vicinity of 1500 L. The work function measurements of Figures 23 and 23 also reach a saturation level in this same neighborhood, near 1800 L. These results differ from those of Zehner and

Gruzalski[37] for the NiAl(110) surface. Their Auger oxygen uptake data indicates that the (110) surface reaches a saturation level at an exposure of 3000 L.

Similarities exist between the bonding of oxygen on NiAl(110) and aluminum. Initially, oxygen will cause an additional XPS peak on aluminum at a binding energy 2 eV higher than the Al 2p peak. This additional peak is due to what is often termed a sub-oxide. After further exposure this peak will shift to 2.4 eV above the Al 2p peak. This peak, as discussed earlier, is due to formation of Al_2O_3. With exposures of 7000 L or more the NiAl(110) surface will form an additional peak with the same energy as the sub-oxide on aluminum. This is evident by looking at the XPS spectra of the Al 2p and Ni 3p core levels shown in Figure 26 and implies the chemical environment on NiAl(110) is similar to that of the sub-oxide which forms on aluminum.

There is no direct interaction between the nickle and adsorbed oxygen, this is evident by referring back to Figure 25. This Figure is a plot of the Ni $2p_{1/2}$ and $2p_{3/2}$ core levels. The only change present in the spectra as a function of exposure is a gradual attenuation of the intensity. Recall, oxidation of nickel will cause the splitting between these peaks to increase. The oxygen adsorbed on the NiAl(110) surface is bonded to the aluminum exclusively. An additional peak at a higher binding energy than the Al 2p peak indicates an oxide is being formed with the aluminum. As discussed above an additional peak forms at an exposure of 7000 L and the peak has a greater amplitude for the 11000L exposure. Further evidence that the oxygen is interacting with the aluminum and not the nickel is given in the Auger spectra of Figure 21. Recall the low energy aluminum and nickel peaks are at 68 eV and 61 eV respectively. The aluminum peak is attenuated faster as a function of exposure. Due to the convolution of these peaks it is not possible to see an additional peak at 51 eV, as would be expected for an aluminum oxide.

Different geometrical or electronic configuration may explain the difference between the positions for Al_2O_3 and the nickel aluminum oxide peaks. Measurements

have been made on the aluminum oxygen bond length in various aluminum oxides with results that range from 1.9 Å to 2.2 Å.[20] The nearest neighbor distance for nickel aluminum is 2.5 Å. Therefore, if the incorporation of oxygen were substitutional in nature the aluminum oxygen bond would exceed that for Al_2O_3. A longer bond length might be associated with less charge transfer which would produce less of a core level shift for oxygen on NiAl(110) than observed in elemental aluminum studies. Alternatively, the nickel in the system could change the valence structure such that less than three electrons are incorporated into the bond. This would also cause less of a shift than for Al_2O_3.

The density of states at the Fermi level for the NiAl(110) is closer to that found in elemental aluminum than that for nickel. Therefore, it is tempting to assume that the chemisorption properties of nickel aluminum would have greater similarities to the oxidation of aluminum than nickel. This idea is supported by the formation of aluminum oxide at high exposures. The presence of nickel reduces the sticking coefficient of oxygen on NiAl(110) to a value significantly lower than for the aluminum surfaces. This reduction in the sticking coefficient is borne out by the studies of aluminum for which saturation coverage is reached for each of the low index faces at ten times less oxygen exposure than we observe for the NiAl(110) surface.

Two of the measurements performed for this study provide about the real-time pictures dynamics of the oxidation process: the Kelvin probe and SHG measurements. Recall in Figure 22, the work function on the clean surface went up dramatically during the initial 30 L of oxygen exposure. The magnitude of this initial increase was about 50 meV. An increase in work function indicates an increase in the surface dipole energy. In the case of oxygen adsorption, which is electronegative, the increase indicates that the oxygen is being adsorbed above the surface. That is, when oxygen dissociates it will localize free electrons from the substrate into the region above the surface. This electron localization will, in turn, increase the work function. For the work function measurement

of Figure 23 made on a contaminated surface shows no initial increase, just a monotonic decrease in the work function. Hence, the initial surface adsorption only occurs on clean surfaces and is a transient effect that occurs before bulk incorporation begins. The localization of electrons should also serve to reduce the nonlinear polarization of the free electrons in the surface and should lead to a decrease in the free electron contribution to the SHG intensity for this system. However, the effect is not observed in the data of Figure 24. This suggests that the non-linear polarizability of this surface is not simply related to the free electron gas model or that the effect is too small to observe within the noise of our measurement.

Further support for the first 30L of oxygen being adsorbed on top of the surface is given by the rippled structure of the NiAl(110) discussed earlier. The aluminum atoms on the clean ordered NiAl(110) surface are relaxed outward and the nickel atoms are relaxed inward. As shown earlier the oxygen bonds to the aluminum on the NiAl(110) surface. This implies for the rippled surface that the preferential bonding sites may be on top of the aluminum atoms.

After the initial increase in the work function shown in Figure 22 the work function decreases steadily. A decreasing work function implies the oxygen is being absorbed below the surface because the subsurface oxygen will produce a negative charge distribution below the surface, thereby introducing a contribution to the surface dipole moment opposite to that of the clean surface. Therefore, the uptake of oxygen is a two stage process initially surface then subsurface. This contrasts the results for Al(111) shown by Erskine and Strong[30], they found for all exposures Al(111) had both surface and subsurface oxygen.

When the oxygen exposure is terminated the work function decreases. Both the magnitude of the work function change and the time over which it occurs is the same as the initial increase. The decrease can be explained in one of two ways: diffusion of oxygen on

the surface into the bulk, or desorption of the surface oxygen. We feel the more likely candidate is surface desorption. Adsorption usually occurs under the following mechanism. First, the oxygen molecules will disassociate on the surface. The atoms will move around until they find an adsorption site or leave the surface. The sticking coefficient is so low on this surface that the rate at which oxygen disassociates on the surface is about equal to the rate that they leave the surface. If the cause of the decrease after the oxygen is removed is surface desorption, there should be similarities between the initial increase and the final decrease. As stated above the similarities are the magnitude and time for the changes to occur. The changes should have the same magnitude, because the cause for the initial increase in work function is reverses after the oxygen is removed.

After the sharp decrease is complete upon removal of the oxygen there is still diffusion occurring. In both measurements presented the work function increases at a slow rate after the decrease. This implies there is.diffusion after the surface desorption. We feel the reason for this is oxygen from the bulk diffusing out towards the surface. The SHG measurements did not exhibit any related behavior during this time, nor was it sensitive to the sharp decrease after the oxygen was removed.

Surface composition information can be obtained for many systems using AES. The following formula[36] is often used to calculate atomic concentrations

$$C_x = \frac{\frac{I_x}{S_x}}{\sum_i \frac{I_i}{S_i}}$$

where I_x is the peak to peak amplitude of element x and S_x is the tabulated[36] elemental sensitivity of element x. These empirically determined elemental sensitivities are tabulated for pure elements. The summation is carried out over one peak per element.

Applying this analysis to the Auger uptake data from Figure 19 yields the results shown in Figure 27. The most notable feature of this figure is that the initial concentration is not 50-50, aluminum-nickel as expected, but 65-35. Hall and Morabito[42] have found that the elemental sensitivities for pure elements must be corrected for alloys. Differences that make this correction necessary between the pure and alloy case are peak shape, atomic density, escape, and backscattering[42]. Calculations to correct for these differences are beyond the scope of this study. Nevertheless we feel that the qualitative information contained in the exposure dependence of the graph is indicative of the main features of the chemisorption process. Notably, there is a larger decrease for aluminum concentration than for the nickel which implies that the oxygen interacts primarily with the aluminum and that nickel serves as a non-bonding bystander. Furthermore, the saturation concentrations 0.52, 0.33, and 0.15 for the aluminum, nickel, and oxygen,respectively, are attained in the 1500 L region.

A second method for calculating the concentrations is to calculate the Auger cross sections using the empirical formulas presented in Chapter 2. We will not be able to use the backscattering correction term because the correction term was empirically derived assuming a pure element base substrate, which is not applicable to alloys. The resulting cross sections for oxygen, aluminum, and nickel are 4.6, 1.0, and 0.66 x 10^{-20} cm^2. The elemental sensitivities as used in the preceding equation are inversely proportional to the cross sections, if no correction is made for mean free path. The resulting sensitivities, with the sensitivity of oxygen normalized to 1, are 1, .22, and .14 for oxygen, aluminum, and nickel respectively. This approach leads to the result that the initial concentration ratio for aluminum to nickel is 20 % to 80 %. The aluminum Auger electrons are almost twice as energetic as those for the nickel, implying the aluminum Auger electrons have a longer mean free path. Correcting these sensitivities for the respective mean free paths will make the initial concentration of aluminum less than 20%. Clearly, this method is

inappropriate for this system but serves to point out the difficulty inherent when one tries to estimate quantitatively atomic concentrations from Auger data for a three atom system.

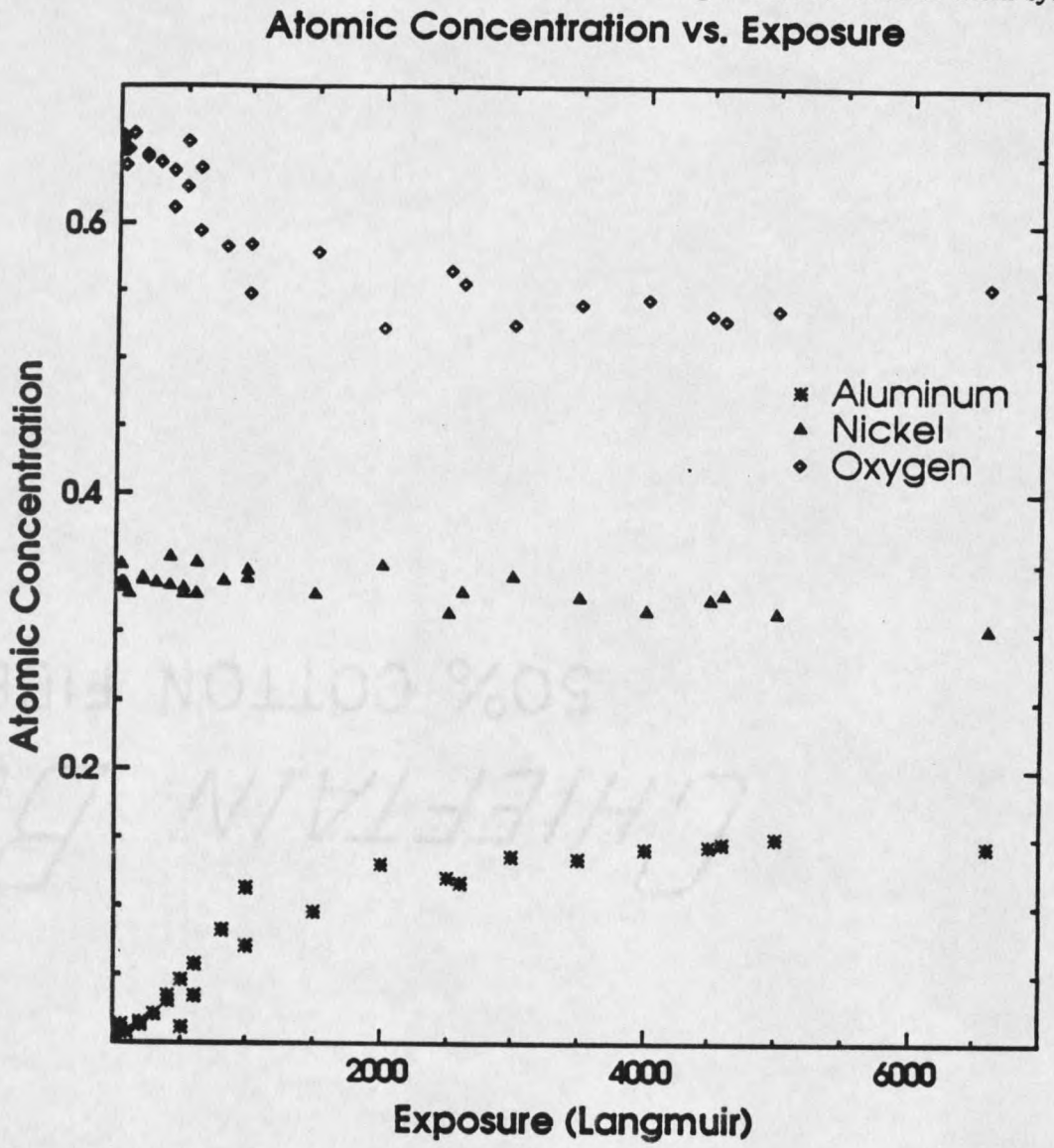

Figure 27: Atomic concentration versus exposure

Relative elemental sensitivities can be obtained from the Auger spectra for the clean surface. First, it is valid to assume that the NiAl(110) surface has equal concentrations of aluminium and nickel because LEED shows a highly ordered surface with the proper symmetry. In this case C_{Al} as computed above will equal C_{NI} when and $S_{Ai} = (I_{Al} / I_{Ni.}) S_{Ni}$. Since, these are relative sensitivities we are free to choose any value for

one of the sensitivities. Choosing $S_{Ni} = 1$ yields a value of .34 for S_{Al} based on the peak heights for a clean surface. This fixes the initial concentration to be 50-50, but does not yield an adjusted sensitivity for oxygen. The choice for the oxygen sensitivity arbitrary and, therefore, the oxygen concentration, is not specified using this approach. Figure 28 is a plot of saturation coverages for a range of choices of oxygen sensitivities. Reading from the Figure, at an oxygen sensitivity of 0.5 the concentration of oxygen is about 0.47; at a sensitivity of 1.5 the concentration is about 0.24. This Figure does not offer any illumination on an appropriate sensitivity for oxygen, but it does draw out one interesting point. Regardless of the value for the oxygen sensitivity there is always a higher concentration of nickel than aluminum. This larger decrease in aluminum supports the model presented earlier that oxygen is adsorbing on top of the aluminum atoms on the surface. Adsorption in this position would block aluminum atoms and result in a higher attenuation of the aluminum signal. This result for the relative concentrations of nickel and aluminum is also supported by the Auger spectra in Figure 21. Recall, these spectra showed a faster and greater attenuation of the aluminum peak height than for the nickel.

A number of conclusions can be drawn from the composition calculations. First the higher concentration of nickle compared to aluminum implies that nickel is remaining a part of the oxide on the surface. This conflicts with Zehner and Gruzalski's[37] analysis and interpretation of the oxidation of the NiAl(110) surface. Their model for adsorption called for diffusion of aluminum atoms to the surface region, with a corresponding decrease in the Auger nickel signal.

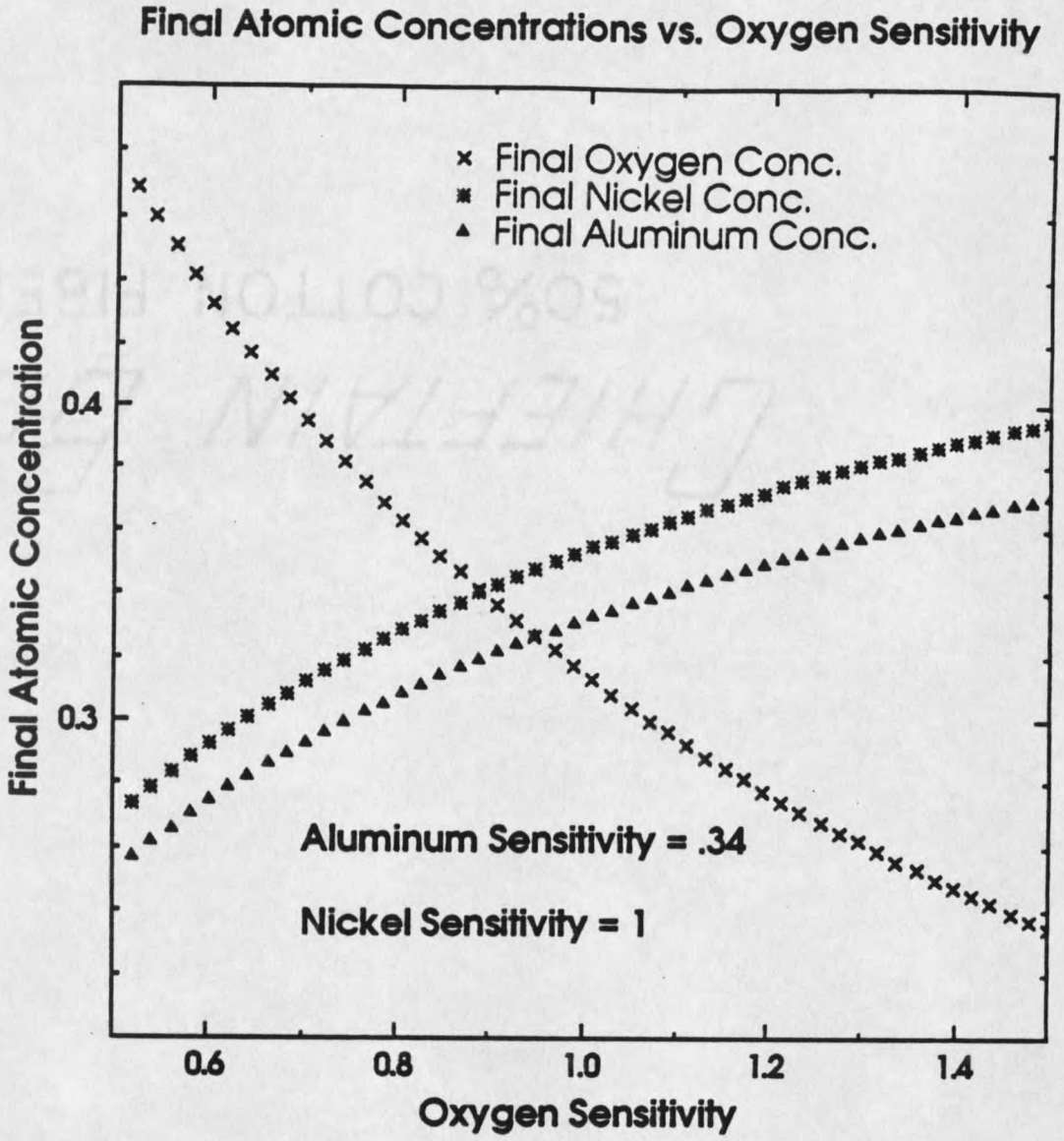

Figure 28: Saturation atomic concentration versus oxygen exposure

REFERENCES CITED

1. C.T. Liu and J.O. Stiegler, Science 226, 636 (1984).
2. C.T. Liu, C.L. White and J.A. Horton, Acta Metall. 33, 213(1985).
3. D.W. Goodman and J.E. Houston, Science 236, 403(1987).
4. C.T. Liu, C.L. White and J.A. Horton, Acta Metall. 33, 231(1985).
5. D. Briggs and M.P. Seah, Practical Surface Analysis, John Wiley and Sons (New York, (1983)
6. E.S.H. Burhop, The Auger Effect and Other Radiationless Transitions, University Press, Cambridge, (1952)
7. H. E. Bishop and J. C. Riviere, J. App. Phys. 40, 1740(1969).
8. C. R. Worthington and S.G. Tomlin, Proc. Phys. Soc. A69, 401(1959).
9. W. Reuter, in Proc. Sixth Int. Conf. on X-ray Optics and Microanalysis, eds G. Shinoda, K. Kohra and T Ichinokawa (Univ. of Tokyo Press, 1972)
10. M. P. Seah and W.A. Dench, Surf. Interface Anal. 1, 2(1979).
11. N.W. Ashcroft and N.D. Mermin, Solid State Physics, Saunders College, Philadelphia, (1976)
12. P.A. Franken, A.E. Hill, C.W. Peters and G Weinreich, Phys. Rev. Letters 7, 118(1961)
13. R. Karplus and J. Swinger, Phys. Rev. 73, 1020(1948).
14. T.F. Heinz, M.M.T. Loy and W.A. Thompson, Phys. Rev. Lett. 54, 63(1985).
15. J.M. Chen, J.R. Bower, C.S. Wang and C.H. Lee, Optics Comm. 9, 132(1983).
16. G.T. Boyd, Y.R. Shen and T.W. Hansch, Optics Lett. 11, 97(1986).
17. N. Bloembergen and P.S. Pershan, Phys. Rev 128, 606(1962).
18. C.K. Chen, T.F. Heinz, D. Ricard and Y.R. Shen, Phys. Rev. Lett. 46, 1010(1981).
19. Y.R. Shen The Principles of Nonlinear Optics, Wiley, New York, London, Sydney, Toronto, (1973)
20. I.P. Batra and L. Kleinman, J. Elect. Spect. Rel. Phen. 33, 175(1984).
21. P. Hofman and A.M. Bradshaw, Surf. Sci. 80, 344(1979).

22. C.D. Wagner, W.M. Riggs, L.E. Davis, J.F. Moulder and G.E. Muilenberg, Handbook of X-Ray Photoelectron Spectroscopy, Perkin-Elmer Corporation, Eden Prairie, (1979)

23. S.H. Flodstrom, C.W.B. Martinson, R.Z. Rachrach, S.B.M. Haystrom and R.S. Bauer, Phys. Rev. Letters 40, 907(1978)

24. A.M.Bradshaw, P. Hofman and W. Wyrobisch, Surf. Sci. 68, 269(1977).

25. R.M. Eastment and C.H.B. Mee, J. Phys. F 3, 1738(1973).

26. W. Eberhardt and F.J. Himpsel, Phys. Rev. Lett. 42, 1375(1979).

27. R. Smoluchowski, Phys. Rev. 60, 661(1941).

28. P.O. Gartland Surf. Sci. 62, 183(1977).

29. R. Michel, J. Gastaldi, C. Allasia and C. Jourdan, Surf. Sci. 95, 309(1980).

30. J.L. Erskine and R.L. Strong, Phys. Rev. B, 25, 5547(1982).

31. R.L. Strong, B. Firey, F.W. de Wette and J.L. Erskine, Phys. Rev. B 26, 3483(1982)

32. P.R. Norton, R.L. Tapping and J.W. Goodale, Surf. Sci. 65, 13(1977).

33. J.E. Demuth and T.N. Rhodin, Surf. Sci. 45, 249(1974).

34. P.H. Holloway and J.B. Hudson, Surf. Sci. 43, 123(1974).

35. S. Evans, J. Pielaszek and J.M. Thomas, Surf. Sci. 56, 644(1976).

36. L.E. Davis, N.C. Macdonald, P.W. Palmberg, G.E. Riach and R.E. Weber. Handbook of Auger Electron Spectroscopy, Perkin-Elmer Corporation, Eden Prairie, (1979)

37. D.M. Zehner and G.R. Gruzalski, in Physical and Chemical Properties of Thin Metal Overlayers and Alloy Surfaces (Eds D.M. Zehner and D.W. Goodman), Materials Research Society, Pittsburgh(1987)

38. S.C. Liu, E.W. Plummer, and D.M. Zehner, p. 191 in National Synchrotron Light Source Annual Report 1986 (BNL 52045), Brookhaven National Laboratory, Upton(1986)

39. A. Taylor and N.J. Doyle, J. App. Cryst.5, 201(1972)

40. J.R. Noonan and H.C. Davis, Phys Rev. Letters 54, 566(1985)

41. S.M. Yalisove and W.R. Graham, Surf. Sci. 183, 556(1987)

42. P.M. Hall and J.M. Morabito, Surf. Sci. 83, 391(1979)

MONTANA STATE UNIVERSITY LIBRARIES
3 1762 10072034 9